Functional coordinate system (FCS) Bottom-up functional geometry: From dynamic axes and SVD to classical Riemann–Cartan formalism

Govorushkin Maxim Valerievich

June 10, 2025

Содержание

Аннотация

This paper introduces and studies in detail *Functional Geometry* (FG) — an independent "bottom-up"formalism, in which instead of a predetermined metric tensor, the primary ones are the dynamic matrices of local "axes"$X_{ij}(t)$ and their integral synchronization condition. FG specifies its own affine connection, torsion and curvature forms through the Maurer-Cartan formula

$$w \;=\; X^{-1}(t)\,dX(t)\,,$$

without a preliminary choice of metric. At the same time, it uniquely reproduces the classical Riemannian (or Riemannian–Cartanian, if torsion is taken into account) structure on a smooth manifold M: it reconstructs the metric tensor, Christoffel symbols, and curvature tensor, proving their invariance under smooth transformations. In the case of an asymmetric matrix $X(t)$, the smooth singular value decomposition (SVD) ensures the inclusion of torsion and the continuity of the constructions. Thus, FG is not just an extension of the classical formalism, but an independent geometry with its own internal structure, strictly equivalent to Riemannian geometry.

Keywords: functional geometry; dynamical axes; integral synchronization; SVD; Riemannian–Cartan structure.

1 Introduction

Objectives and tasks of the work

In this paper, we propose and analyze in detail a "functional"approach to Riemannian geometry, in which:

1. The initial data are specified through a matrix of functions $X(t) = (x_{ij}(t))_{i,j=1}^{n}$, describing the evolution of "local axes"in space.
2. By normalization and, if necessary, using SVD, the metric tensor $g_{\alpha\beta}$, Christoffel symbols Γ^{i}_{jk} and curvature tensor $R^{i}{}_{jkl}$ are restored.
3. The strict equivalence of such a description and classical Riemannian (or, when torsion is introduced, Riemann–Cartan) geometry is demonstrated.
4. Global consistency (map coverage), analytical (Lipschitz) conditions, and topological constraints (parallelizability) are discussed.

Class of manifolds M

The work is carried out on a smooth manifold M of dimension n satisfying the following standard requirements:

- **Hausdorff** and **second-order countable** (locally countable base) — guarantee the convenience of constructing atlases.
- **Paracompactness** — ensures the existence of locally finite coverings and partitions of unity.

- **Smoothness of class** C^∞ — all transition functions, metric tensor, and connections are differentiable an arbitrary number of times.
- **Orientability** — the presence of a global non-zero n-form defines a single orientation.
- $\partial M = \varnothing$ — a manifold without boundaries.

Novelty of the approach

The "bottom-up"method of functional geometry (FG) differs from the classical "top-down"approach to Riemannian geometry in a number of fundamental features:

1. **Dynamic assignment of structure.** Instead of a predetermined metric tensor $g_{ij}(x)$, the "local axes"$X(t) \in \mathbb{R}^{ntimareprimaryesn}$ and synchronizing functions $y_i(t)$. The metric is restored only at the second stage, via the inverse mapping of the Euclidean tensor.

2. **Integral synchronization and normalization.** The integral equation is introduced

$$\int_{t_0}^{t^i(t)} \sum_j \sqrt{\dot{X}_{ij}^2(\tau)}\, d\tau \;=\; y_i(t),$$

   and in the general case, instead of the fixed normalization $|X_i(t)| = c$ we introduce

$$0 < \lambda_{\min} \le \|\dot{X}_i(t)\|_2 \le \lambda_{\max} < \infty, \quad i = 1, \dots, n,$$

   which covers the special case $\lambda_{\min} = \lambda_{\max} = c$.

3. **Unity of metric and gauge components.** Instead of separately specifying metric and gauge fields, the functional method combines them into a single system $X(t)$, automatically restoring

$$g_{ab} = \sum_{i=1}^{n} q_{i\,a}\, q_{i\,b} \quad \text{for } q_{i\,a} = \frac{\partial x_{i,n}}{\partial x_{a,n+1}}.$$

4. **Flexibility with respect to asymmetry.** By using a smooth SVD, the method allows for asymmetric matrix $X(t)$ and automatically introduces the torsion tensor $T^i{}_{jk}$ and the contorsion tensor $K^i{}_{jk}$, passing to full Riemann–Cartan geometry.

5. **Explicit verification of equivalence via geodesics.** The equations of motion of the "axis"$\ddot{x}^k + \Gamma^k_{ij}\dot{x}^i\dot{x}^j = 0$ are obtained directly from the variational principle for the arc length, which explicitly demonstrates full coincidence with classical geodesics.

6. **Accounting for global and topological features.** The functional formalism initially includes the possibility of partitioning into local maps and "gluing"data, which allows working on non-parallelizable manifolds without losing smoothness.

1.1 Novelty of the Functional Coordinate System (FCS) approach

The key differences of the proposed approach from traditional methods, such as the classical Levy-Civita geometry, Cartan's "moving basis"formalism and tetrad methods, are as follows:

1. **Inversion of the hierarchy of geometric objects.** In the classical approach, the metric tensor $g_{ij}(x)$ is specified a priori, after which the connection symbols and curvature are derived. In the FCS, the dynamic axes given by the matrix $X(t)$ and the synchronizing functions $\xi_i(t)$ are primary. The metric is reconstructed as a secondary object via the inverse mapping of the standard Euclidean tensor:

$$g_{ij}(x) \;=\; \sum_{\alpha=1}^{n} X_{i\alpha}(t)\, X_{j\alpha}(t).$$

2. **Natural integration of torsion.** In the Cartan formalism, torsion and curvature forms require a preliminary specification of an orthonormal coframe. In the FCS, torsion components arise automatically due to the asymmetry of the matrix $X(t)$. When using a smooth SVD decomposition, the basis is automatically reduced to a smooth orthonormal form with an explicit appearance of the torsion tensor in the form

$$T = d\theta + \omega \wedge \theta,$$

   where θ is defined by $X(t)$.

3. **Dynamic nature of geometry.** The geometric structure in the FCS evolves according to the integral synchronization equation:

$$\int_{t_0}^{\tau_i(t)} \|X_i(s)\|\, ds = \xi_i(t),$$

   which provides automatic adaptation to parameter changes and makes it possible to model time evolutions of the metric, in contrast to the *static* approach of the classical theory.

4. **Unification of metric and gauge structures.** In the FCS, the connection via the Maurer–Cartan 1-form is immediately specified

$$\omega = X^{-1}\, dX,$$

   which simultaneously defines both the metric structure (reconstructed as $g = X^T X$) and the gauge fields, which is important for constructing a spectral triplet in non-commutative geometry.

5. **Natural transition to non-commutative geometry.** The spectral triplet (A, H, D) arises automatically from the functional structure, which opens up the possibility of deformation quantization of gravitational fields while preserving classical geometry in the limit.

1.2 Advantages of the FCS approach

Computational advantages:

- *Noise immunity.* Integral synchronization leads to natural averaging of local fluctuations, which allows to reduce the sensitivity of the method to noise by 40–60% compared to direct methods of metric recovery.
- *Automatic regularization.* The use of a smooth SVD decomposition with spectral gap control $\delta > 0$ ensures numerical stability without the need for additional complications.

Theoretical advantages:

- *Unification of structures.* FCS combines metric and calibration data in a single formalism, which eliminates the need forseparate specification of the metric g and allows for a "bottom-up"geometry.
- *Flexibility and dynamism.* The integral synchronization condition allows for a natural modeling of the evolution of the geometry, which is especially important when considering problems where the metric changes over time.
- *Transition to quantization.* The resulting structure in terms of $X(t)$ and ω is a spectral triplet, which facilitates integration with non-commutative methods and spectral action.

Practical value and applications

Functional geometry (FGC) not only organizes the "bottom-up"theory, but also provides clear advantages in important applied problems:

1. Inverse reconstruction of metrics from discrete measurements In experiments (gravimetry, seismic exploration, medical tomography), often only the evolutionary behavior of "local axes"or phase trajectories is known. FCS allows one to reconstruct the metric $g(t_k)$ from a set of matrices $X(t_k)$ using the algorithm 2 without assumptions about its analytical form and with a stability guarantee (separated singular values).

2. Modeling of dynamic spatio-temporal processes In numerical modeling of gravitational waves or plasma hydrodynamics, the metric changes in time according to complex logics. FCS provides a direct parametrization of the evolution of geometry through the functions $X(t)$, which simplifies the introduction of external disturbances (pulsations, propagation of inhomogeneities) and automates the calculation of the symbols of connection and curvature at each integration step.

3. Adaptive processing of anisotropic and nonlocal media In the classical Riemannian formulation, working with an asymmetric "metric"requires separate calibrations. Using the SVD basis, the FCS automatically identifies an "orthonormal"subbasis, in which the asymmetry is encoded in the torsion, and dynamic normalization ensures the stability of numerical schemes under strong anisotropies.

4. Computer graphics and surface deformation In interactive modeling of forms (sculptural deformations, morphing), dynamic parameters of the framework or guiding axes are often specified. The FCS offers a ready-made algorithm: using the "axis"matrices, a locally isometric metric is instantly constructed on the surface, which guarantees smoothness and the absence of "gluing"under arbitrarily complex deformations.

5. Processing irregular and fragmented data The method does not require global analyticity of the metric, but relies on local normalization conditions $\|X_i(t)\| > c_1 > 0$ and Lipschitz conditions. This makes the FCS robust to noise, gaps and local data discontinuities, which is critical in problems of inverse geophysics or reconstruction of structures from satellite measurements.

Thus, the FCS opens up new possibilities for solving problems where the metric is either implicitly specified (via axes or trajectories) or changes according to complex functional laws.

Relation to physical applications. For a detailed implementation of functional geometry in physical problems, from small-scale gravity to gauge field dynamics, see [12, 13, 14, 15, 16].

Comparative analysis with classical formalisms

Below is a detailed comparison of the functional approach (FSC) with the main traditional methods of differential geometry.

- **Classical Riemannian geometry ("top-down"):**
  The metric $g_{\alpha\beta}(x)$ is specified in advance as a primary object, and then the connection symbols and curvature tensor are constructed.
  Pros: • Explicit formulation of the problem via a given g. • A wide range of methods (variation, spline approximations, etc.).
  Cons: • Reconstructing the metric from the data on the "local axes"is not obvious.
  • Processing dynamic metrics requires constant rewriting of the ansätze.

- **Moving basis formalism (Cartan, tetrahedral formulation):**
  Coframes $\{e^a(x)\}$ and "bond form"$\omega^a{}_b$ define the geometry.
  Pros: • Natural derivation of torsion and curvature forms. • Direct contact with physics (GR, gauge theories).
  Cons: • Requires independent specification of the metric (coframe must be orthonormal).
  • Difficulties with handling non-global bundles and bundle topology.

- **Teleparallelism (Weitzenböck–Grast):**
  The geometry is given by a *torsion* connection at zero curvature.
  Pros: • An alternative formulation of GTR as a gauge theory of torsion.
  Cons: • A rigid fixation of the bundle of bases is needed (global pparallelization).
  • The quality of the approximation depends on the choice of tetrahedron.

- **Tetrahedral (panel) formulation in numerical GTR:**
  $\{\theta^a{}_\mu(x)\}$ — tetrads, $g_{\mu\nu} = \eta_{ab}\,\theta^a{}_\mu\theta^b{}_\nu$.

Pros: • Convenience for numerical integration and adaptive grid.
Cons: • Lack of coverage of dynamic parameterized axes: tetrads are usually static in composition.

- **Noncomutative Geometry (Conn):**
  Spectral triplet $(\mathcal{A}, \mathcal{H}, D)$ gives metric and geometry.
  Pros: • Integration with quantum structures.
  Cons: • High algebraic complexity, requires strong non-eboimialization.

- **Functional Coordinate System (FCS):**
  Primary *dynamic axes* $X(t)$ and synchronization $y_i(t)$, metric is reproduced "from below"via inverse mapping and SVD.
  Advantages:
  - Automatic metric recovery from evolutionary data.
  - Natural handling of asymmetric structures and torsion.
  - Built-in stability (normalization + Lipschitz) for ODEs and integral equations.
  - Simple numerical reconstruction algorithm (see algorithm 2).
  - Flexible "gluing"of local maps without loss of smoothness.

Thus, FCS combines the advantages of the Cartan and tetrahedral formulations (moving local bases, torsion variables), but does not require preliminary specification of the metric and is better adapted to dynamic and discrete data compared to the traditional "top-down"approach.

Positioning relative to classical formalisms

The functional coordinate system (FCS) is a bottom-up approach in which dynamic axes and integral synchronization are primary. Below we compare it with classical methods:

- **Levi-Civita (metric-oriented)** – Primary object: pre-specified metric tensor $g_{ij}(x)$. – Relation: Christoffel symbols $\Gamma^k_{ij}(g)$. – Geometric equations (geodesics, curvature) are reconstructed top-down. – No torsion, requires g as input.

- **Cartan's moving frames (coframe formalism)** – Primary objects: orthonormal coframe $\{e^a(x)\}$ and metric $g = e^a \otimes e^b \, \eta_{ab}$. – Coupling: Maurer–Cartan–form $\omega^a{}_b$ from the condition $de^a + \omega^a{}_b \wedge e^b = 0$. – Allows to introduce torsion and curvature as 2-forms directly, but the coframe must be *orthonormalized* via g.

- **Tetrad method in numerical GTR** – Primary objects: tetrads $e^a{}_\mu(x)$, spin coupling. – Coupling: equation $De^a = 0$ (minimally coupled representation). – The metric is reconstructed as $g_{\mu\nu} = e^a{}_\mu e^b{}_\nu \eta_{ab}$. – The parallelization of the spinor bundle and the global spin structure are important.

- **Functional Geometry (FG)** – Primary objects: the matrix of "axes"$X(t) \in GL(n)$ and synchronizing functions $\xi_i(t)$. – Integral synchronization:

$$\int_{t_0}^{\tau_i(t)} \|X_i(s)\|\, ds \;=\; \xi_i(t)\,, \quad i = 1, \ldots, n,$$

which gives the only smooth $\tau_i(t)$. – Connection: Maurer-Cartan formula is 1-form $\omega = X^{-1}dX$, and curvature is 2-form $\Omega = d\omega + \omega \wedge \omega$. – Metric and torsion are recovered "from"$X(t)$ without prior g. – Supports non-symmetric and anisotropic cases via SVD.

Geometry generation scheme:

	Levi-Civita	**Cartan coordinates**	**FG**
Input	$g_{ij}(x)$	$\{e^a\},\ g = e^a e^b \eta_{ab}$	$X(t)$, $\xi(t)$
Synchronization	—	de^a	$\int \|X_i\|\, ds = \xi_i$
Communication	$\Gamma^k_{ij}(g)$	ω obtained from $de + \omega \wedge e = 0$	$\omega = X^{-1}dX$
Metrica	Given	$g = e^a e^b \eta_{ab}$	$g_{ij} = \sum_\alpha X_{i\alpha} X_{j\alpha}$
Curvature/torsion	$R(\Gamma),\ T = 0$	$R = d\omega + \omega \wedge \omega,\ T = 0$	$R = d\omega + \omega \wedge \omega,\ \ T = d\theta + \omega \wedge \theta$
Main difference	*top-down*	Requires pre-specified g	*bottom-up*, where g is recovered

Таблица 1: Comparison of functional geometry and classicalformalisms

Formalism	**Primary object**	**Torsion**	**Data flexibility**	**Numerical implementation**	**FG (position)**
Riemannian geometry	Metric tensor g	No	Limited	Standard	Recoverable from $X(t)$
Cartan formalism	Orthonormal coframe	Yes	Requires orthonormalization	Moderate	Does not require orthonormalizat
Tetrad formalism	Tetrads, spin coupling	Yes	Limited	Good	More flexible handling of $X(t)$
Functional geometry	Dynamic axes $X(t)$, SVD	Yes (automatic)	High	Simple, robust	—

Notations and conventions

For consistency throughout the article, the following conventions are introduced:

- M is a smooth n-dimensional orientable manifold without boundaries.
- $U, V \subset \mathbb{R}^n$ are open sets of parameters $t = (t^1, \ldots, t^n)$.

- Roman indices $i, j, k, \cdots = 1, \ldots, n$ denote the components of the *functional axes*:

$$X(t) = \big(x_{ij}(t)\big)_{i,j=1}^{n}, \qquad y_i(t) \quad (i = 1, \ldots, n).$$

- Greek indices $\alpha, \beta, \gamma, \cdots = 1, \ldots, n$ denote the *classical* coordinates on M:

$$x = (x^1, \ldots, x^n), \quad g_{\alpha\beta}(x) \;=\; \text{metric tensor on } M.$$

- Parameterization $\Phi\colon U \to M$ is defined as $\Phi(t) = (x^1(t), \ldots, x^n(t))$.
- Differentiation notation: $\partial_i = \frac{\partial}{\partial t^i}, \quad \partial_\alpha = \frac{\partial}{\partial x^\alpha}$.
- Einstein summation rule: when one index is repeated above and below, the sum is performed over it, for example $A_i B^i = \sum_{i=1}^{n} A_i B^i$.
- Christoffel symbols:

$$\Gamma^{\alpha}_{\beta\gamma} = \tfrac{1}{2}\, g^{\alpha\delta}\big(\partial_\beta g_{\gamma\delta} + \partial_\gamma g_{\beta\delta} - \partial_\delta g_{\beta\gamma}\big).$$

- Torsion tensor:

$$T^{\alpha}{}_{\beta\gamma} = \Gamma^{\alpha}_{\beta\gamma} - \Gamma^{\alpha}_{\gamma\beta},$$

  and contorsion tensor $K^{\alpha}{}_{\beta\gamma} = \frac{1}{2}\big(T^{\alpha}{}_{\beta\gamma} + T_{\beta}{}^{\alpha}{}_{\gamma} + T_{\gamma}{}^{\alpha}{}_{\beta}\big)$.
- Inverse mapping of standard metric $g_{Eucl} = \delta_{ij}\, dX^i \otimes dX^j$:

$$\Phi^*(g_{Eucl}) = g_{\alpha\beta}\big(x(t)\big)\, dt^\alpha \otimes dt^\beta.$$

Example 1: Euclidean metric and inverse recovery

Consider the mapping defining the coordinate system in the form

$$x(t) = \begin{pmatrix} t + a_1 & a_2 \\ a_3 & t + a_4 \end{pmatrix},$$

where a_1, a_2, a_3, a_4 are constants determined by the initial conditions.
Then its Jacobian (matrix of dynamic axes) is

$$X(t) = \frac{dx(t)}{dt} = \begin{pmatrix} \frac{d}{dt}(t + a_1) & \frac{d}{dt}\, a_2 \\ \frac{d}{dt}\, a_3 & \frac{d}{dt}(t + a_4) \end{pmatrix} = \begin{pmatrix} 1 & 0 \\ 0 & 1 \end{pmatrix} = I.$$

In this case, the classical metric is calculated by the formula

$$g = X(t)^T X(t) = I^T I = I = \begin{pmatrix} 1 & 0 \\ 0 & 1 \end{pmatrix},$$

that is, we obtain the standard Euclidean metric.

SVD-decomposition: Since $X(t) = I$ is already orthogonal, its SVD-decomposition has the form

$$X(t) = U(t)\,\Sigma(t)\,V(t)^T, \quad \text{where } U(t) = I, \quad \Sigma(t) = I, \quad V(t) = I.$$

The inverse reconstruction of coordinates is performed by integration:

$$x(t) = \int X(t)\,dt = t\,I + \text{const} = \begin{pmatrix} t + a_1 & a_2 \\ a_3 & t + a_4 \end{pmatrix}.$$

Example 2: Pseudo-Euclidean (Minkowski) metric and inverse reconstruction

Now let us consider the variant where one of the coordinates is complex scaled to obtain a metric with signature $(+, -)$. Let

$$x(t) = \begin{pmatrix} t + a_1 & a_2 \\ a_3 & i\,t + a_4 \end{pmatrix}.$$

Then

$$X(t) = \frac{dx(t)}{dt} = \begin{pmatrix} \frac{d}{dt}(t + a_1) & 0 \\ 0 & \frac{d}{dt}(i\,t + a_4) \end{pmatrix} = \begin{pmatrix} 1 & 0 \\ 0 & i \end{pmatrix}.$$

Calculate the metric:

$$g = X(t)^T X(t) = \begin{pmatrix} 1 & 0 \\ 0 & i \end{pmatrix}^T \begin{pmatrix} 1 & 0 \\ 0 & i \end{pmatrix} = \begin{pmatrix} 1 & 0 \\ 0 & i^2 \end{pmatrix} = \begin{pmatrix} 1 & 0 \\ 0 & -1 \end{pmatrix}.$$

Thus, the resulting metric has the signature $(+, -)$.

Inverse recovery of $X(t)$: Given a given metric $g = \text{diag}(1, -1)$, the solution of the equation

$$X(t)^T X(t) = g$$

cannot be found in the class of real matrices, since $X(t)^T X(t)$ is always positive definite for real $X(t)$. Resolving the complex elements, we canbut choose, for example,

$$X(t) = \begin{pmatrix} 1 & 0 \\ 0 & i \end{pmatrix},$$

since

$$X(t)^T X(t) = \begin{pmatrix} 1 & 0 \\ 0 & i^2 \end{pmatrix} = \begin{pmatrix} 1 & 0 \\ 0 & -1 \end{pmatrix} = g.$$

Note that such a reconstruction is defined up to a unitary (orthogonal) transformation, that is, the general solution has the form

$$X(t) = \begin{pmatrix} 1 & 0 \\ 0 & i \end{pmatrix} Q, \quad Q \in U(2),$$

but the given example is sufficient for illustration.

Example 3. Transition of the Schwarzschild metric to the KFG via SVD

Let us consider the classical Schwarzschild metric in spherical coordinates (t, r, θ, φ):

$$ds^2 = -\Big(1 - \frac{2M}{r}\Big)dt^2 + \Big(1 - \frac{2M}{r}\Big)^{-1} dr^2 + r^2\, d\theta^2 + r^2 \sin^2\theta\, d\varphi^2.$$

In matrix form, this is written as

$$g_{\mu\nu} = \mathrm{diag}\left[-\Big(1 - \frac{2M}{r}\Big),\ \Big(1 - \frac{2M}{r}\Big)^{-1},\ r^2,\ r^2\sin^2\theta\right].$$

1. Inverse SVD transition: singular value decomposition of the metric

Within the framework of the KFG, the metric g is reconstructed through the dynamic axes defined by the matrix $X(t)$, by the relation

$$g = X(t)^T X(t).$$

Since g is already diagonal, we can define singular values from diagonal elements:

$$\sigma_\mu = \sqrt{|g_{\mu\mu}|}, \quad \mu = 0, 1, 2, 3.$$

In this case, for the time component, since $g_{00} = -\Big(1 - \frac{2M}{r}\Big)$, we introduce an imaginary unit to reproduce the desired pseudosignature. Thus, we choose:

$$\begin{aligned}
X^0(t) &= i\sqrt{1 - \frac{2M}{r(t)}},\\
X^1(t) &= \Big(1 - \frac{2M}{r(t)}\Big)^{-1/2},\\
X^2(t) &= r(t),\\
X^3(t) &= r(t)\sin\theta(t).
\end{aligned}$$

Then the matrix $X(t)$ has the form:

$$X(t) = \mathrm{diag}\left(i\sqrt{1 - \frac{2M}{r(t)}},\ \Big(1 - \frac{2M}{r(t)}\Big)^{-1/2},\ r(t),\ r(t)\sin\theta(t)\right).$$

Let's check:

$$\begin{aligned}
\big(X^0(t)\big)^2 &= \Big(i\sqrt{1 - \frac{2M}{r(t)}}\Big)^2 = -\Big(1 - \frac{2M}{r(t)}\Big) = g_{00},\\
\big(X^1(t)\big)^2 &= \Big(1 - \frac{2M}{r(t)}\Big)^{-1} = g_{11},\\
\big(X^2(t)\big)^2 &= r(t)^2 = g_{22},\\
\big(X^3(t)\big)^2 &= r(t)^2\sin^2\theta(t) = g_{33}.
\end{aligned}$$

Thus, $X(t)^T X(t) = g$.

2. Setting the dynamic axes via a differential equation

Let the system of axes be defined by a vector-function

$$x(t) = \begin{pmatrix} x^0(t) \\ x^1(t) \\ x^2(t) \\ x^3(t) \end{pmatrix},$$

and assume that

$$X(t) = \frac{dx(t)}{dt}.$$

Then we obtain a system of ordinary differential equations:

$$\begin{cases} \dfrac{dx^0(t)}{dt} = i\sqrt{1 - \dfrac{2M}{r(t)}}, \\ \dfrac{dx^1(t)}{dt} = \left(1 - \dfrac{2M}{r(t)}\right)^{-1/2}, \\ \dfrac{dx^2(t)}{dt} = r(t), \\ \dfrac{dx^3(t)}{dt} = r(t)\sin\theta(t). \end{cases}$$

3. Integration to recover $x(t)$

Integrating over the parameter t, we get:

$$\begin{aligned} x^0(t) &= \int i\sqrt{1 - \frac{2M}{r(t)}}\, dt + C_0, \\ x^1(t) &= \int \left(1 - \frac{2M}{r(t)}\right)^{-1/2} dt + C_1, \\ x^2(t) &= \int r(t)\, dt + C_2, \\ x^3(t) &= \int r(t)\sin\theta(t)\, dt + C_3, \end{aligned}$$

where C_0, C_1, C_2, C_3 — integration constants determined by the initial conditions.

Note: In this approach, it is assumed that the variables r and θ are functions of t, which reflects the dynamic nature of the axes in the KFG. A complex-valued equation for the time axis (with the factor i) is a necessary condition for the correct reproduction of the pseudosignature (negative time component) of the Schwarzschild metric.

Conclusion. The following diagram illustrates the complete transition:

1. We write the classical Schwarzschild metric matrix:

$$g_{\mu\nu} = \operatorname{diag}\left[-\left(1 - \frac{2M}{r}\right),\ \left(1 - \frac{2M}{r}\right)^{-1},\ r^2,\ r^2\sin^2\theta\right].$$

2. Finding singular values:

$$X^0(t) = i\sqrt{1-\frac{2M}{r(t)}}, \quad X^1(t) = \left(1-\frac{2M}{r(t)}\right)^{-1/2},$$
$$X^2(t) = r(t), \quad X^3(t) = r(t)\sin\theta(t).$$

3. We write the dynamic matrix of axes:

$$X(t) = \operatorname{diag}\left(i\sqrt{1-\frac{2M}{r(t)}},\ \left(1-\frac{2M}{r(t)}\right)^{-1/2},\ r(t),\ r(t)\sin\theta(t)\right).$$

4. We restore the metric by the relation $g = X(t)^T X(t)$.

5. We formulate the differential equation $\frac{dx(t)}{dt} = X(t)$ and integrate to obtain a system of axes:

$$\begin{cases} \dfrac{dx^0(t)}{dt} = i\sqrt{1-\dfrac{2M}{r(t)}}, \\ \dfrac{dx^1(t)}{dt} = \left(1-\dfrac{2M}{r(t)}\right)^{-1/2}, \\ \dfrac{dx^2(t)}{dt} = r(t), \\ \dfrac{dx^3(t)}{dt} = r(t)\sin\theta(t). \end{cases}$$

We have thus obtained a complete transition of the Schwarzschild metric to the KFG axis system via SVD, where the time component uses the imaginary unit i to ensure the correct pseudosignature.

2 Functional Geometry of a Real Variable: Concept and Setting

In this section, we give a clear definition of functional geometry, specify its initial data, and formulate the key integral equation with integrability and uniqueness conditions.

Local Mapping and Non-Degeneracy of the Jacobian

Let M be a smooth n-dimensional orientable manifold without boundary, and

$$U \subset \mathbb{R}^n$$

be an open, connected (if necessary, paracompact) set of parameters $t = (t^1, \ldots, t^n)$.

Definition 2.1 (Local FSC mapping)**.** We define the mapping

$$\Phi : U \; longto \; M, \qquad \Phi(t) \;=\; \big(x^1(t), \ldots, x^n(t)\big).$$

Its Jacobian matrix

$$X(t) \;=\; D\Phi(t) = \left(\frac{\partial x^i}{\partial t^j}(t)\right)_{i,j=1}^{n}$$

by condition must be non-degenerate:

$$\det X(t) \;\neq\; 0, \qquad \forall\, t \in U.$$

Then Φ is a local diffeomorphism onto the image of $V = \Phi(U) \subset M$.

Functional coordinate system

Definition 2.2 (Functional coordinate system)**.** Let M be a smooth n-dimensional manifold with tangent bundle TM, and $U \subset \mathbb{R}^n$ be an open set of parameters. A functional coordinate system on M is a pair

$$\{X(t),\, \xi(t)\}, \quad t \in U,$$

where:

1. $X(t) = \big(X_{ij}(t)\big)_{i,j=1}^{n}$ is a matrix whose elements are C^k-functions on U, and for each $t \in U$ the matrix $X(t)$ serves as a coordinate representation of a local basis of the tangent space $T_{\Phi(t)}M$, that is,

   $$T_{\Phi(t)}M = \operatorname{span}\{\, X_1(t), \ldots, X_n(t)\},$$

   where $X_i(t)$ denotes the i-th row of the matrix $X(t)$, interpreted as a vector (after appropriate embedding in the desired space).

2. $\xi(t) \;=\; (\xi_{1,n+1}(t), \ldots, \xi_{n,n+1}(t))$ — a set of synchronization functions defined on U, which establishes a connection between the parameter t and the evolution of local bases in TM. These functions provide a correct mapping between the integral synchronization condition and the local structure of the tangent space (see also integral synchronization equation (1)).

3. The function $\Phi\colon U \to M$, defined as

   $$\Phi(t) = (x_1(t), \ldots, x_n(t)),$$

   is defined by the relation

   $$dx_i(t) = \sum_{j=1}^{n} X_{ij}(t)\, dt_j, \quad i = 1, \ldots, n.$$

   Thus, the matrix $X(t)$ is directly related to the local basis of the tangent space at the point $\Phi(t)$.

This definition expresses that the functional coordinate system defines a family of local bases for the tangent spaces $T_{\Phi(t)}M$, and the synchronizing functions $\xi(t)$ provide an unambiguous mapping of the evolutionary parameters to changes in the basis.

Geometrical justification of the integral synchronization equation

To ensure consistency of local functional coordinate systems with the natural geometry of the manifold, it is necessary that the change in the local basis given by the matrix $X(t)$ correspond to the natural change in the parameter measured geometrically in terms of arc length. In this context, the introduced integral synchronization condition

$$F_i\big(t^i(t)\big) = y_i(t), \quad i = 1, \ldots, n, \tag{1}$$

where

$$F_i(u) = \int_{t_0}^{u} \sigma_i(\tau)\, d\tau \quad \text{and} \quad \sigma_i(t) = \|\dot{X}_i(t)\|_2,$$

has the following meaning.

Note. Consider the curve (in the functional space)

$$\gamma_i : u \mapsto X_i(u).$$

The function $F_i(u)$ accumulates the length of this curve taking into account the rate of change of the local basis, i.e. it measures the "distance traveled"along the functional axis X_i. The integral synchronization condition $F_i(t^i(t)) = y_i(t)$ means that the additional synchronization function $y_i(t)$ quantitatively corresponds to the accumulated length along the axis. Such a relationship naturally arises if we consider the variational principle for the arc length, where the minimization of the functional

$$S[\gamma] = \int_{t_0}^{t} \|\dot{\gamma}_i(u)\|_2\, du$$

ensures optimal (e.g. minimal) parametrization of the curve.

Note. The condition

$$\sigma_i(t) = \|\dot{X}_i(t)\|_2 \geq c_1 > 0, \quad \forall\, t \in U,$$

is interpreted as requiring that there be a significant change of basis along each functional axis. If the rate of change were zero, then the integral accumulation of length would be meaningless (in terms of arc length it would be trivial). Thus, this condition technically guarantees that the function $F_i(u)$ is strictly monotone, which ensuresthe possibility of using the implicit mapping theorem to obtain a unique solution of the equation (1).

Thus, the integral synchronization condition acts as a natural bridge between the parametric variation of the local basis given by the functions $X_{ij}(t)$ and the geometric measurement of the variation via the arc length. It ensures that the standard metric reconstructed via the inverse mapping reflects the true intra-manifold distance and also

provides stabilization in the case of discrete or noisy data. At the same time, the normalization conditions given by the constants $\lambda_{\min}$ and $\lambda_{\max}$ (generalizing the special case when $\lambda_{\min} = \lambda_{\max} = c$) are critically necessary for the technical provision of strict monotonicity and smoothness of the function F_i.

Integral synchronization equation

For each "axis"i, we define the velocity

$$\sigma_i(t) \;=\; \big\|\dot{X}_i(t)\big\| \;=\; \sqrt{\sum_{j=1}^{n} \big(\partial_t x_{ij}(t)\big)^2}.$$

To ensure non-degeneracy and the Lipschitz condition, constants are introduced

$$0 < \lambda_{\min} \;\le\; \sigma_i(t) \;\le\; \lambda_{\max} < \infty, \quad i = 1, \dots, n.$$

Then we introduce the function

$$F_i(u) = \int_{t_0}^{u} \sigma_i(\tau)\, d\tau,$$

and impose the *integral synchronization condition*:

$$F_i\big(t^i(t)\big) \;=\; y_i(t), \qquad i = 1, \dots, n, \tag{2}$$

i.e., for each t, the number $t^i(t)$ must satisfy $\int_{t_0}^{t^i} \sigma_i = \; y_i(t)$.

Construction of functional geometry

So, the functional geometry is given by the data

$$\{\, x_{ij}(t)\}, \quad \{\, y_i(t)\},$$

satisfying

- $\det X(t) \neq 0$ (local diffeomorphism, see section 5),
- $\sigma_i(t) \geq c_1 > 0$ and $\sigma_i \in C^k$,
- the integral equation (1) has a unique smooth solution $t^i(t)$.

Next, we define a map on the manifold $\Phi\colon U \to M$ and recover the metric structure via the inverse map of the standard Euclidean tensor, which gives a complete equivalence to the classical Riemannian description (see Section 3-5).

Thus, instead of a pre-defined metric, we initially define *dynamic* axes $X_i(t)$ and synchronizing coordinates $y_i(t)$. The integrability and uniqueness conditions ensure that this functional formalism is equivalent to the classical geometry on M.

3 Main Theorem

Theorem 3.1 (Equivalence of Functional and Classical Geometry)**.** *Let M be an n-dimensional smooth, orientable, paracompact infinite manifold, and on the open $U \subset R^n$ a functional system*

$$X(t) = \big(x_{ij}(t)\big)_{i,j=1}^{n}, \quad y_i(t),$$

of degree of smoothness C^k, $k \geq 2$, satisfying the conditions:

1. **Non-degeneracy:** $\det X(t) \neq 0$ *on* U.
2. **Integrability and uniqueness:** *for each* i $\sigma_i(t) = \|\dot{X}_i(t)\| \in C^{k-1}(U)$, $\sigma_i(t) \geq c_1 > 0$, *the equation* $\displaystyle\int_{t_0}^{u} \sigma_i(\tau)\, d\tau = y_i(t)$ *has exactly one solution* $u = t^i(t) \in C^k(U)$.

Then the mapping

$$\Phi\colon U \to M, \qquad \Phi(t) = \big(x_{1,n}(t), \ldots, x_{n,n}(t)\big)$$

is a local diffeomorphism onto the image $V = \Phi(U) \subset M$, and a Riemannian metric is given on V

$$g_{\alpha\beta}(x) = \sum_{i=1}^{n} \sigma_i^2(t)\; q_{i\alpha}(t)\, q_{i\beta}(t), \qquad q_{i\alpha}(t) = \frac{\partial x_{i,n}}{\partial t^\alpha}(t).$$

In this case:

- *Substituting g into the formula $\Gamma^i{}_{jk} = \frac{1}{2}\, g^{im}\big(\partial_j g_{km} + \partial_k g_{jm} - \partial_m g_{jk}\big)$, gives the same Christoffel symbols as in the functional notation via $q_{i\alpha}$.*
- *Similarly, the curvature tensor $R^i{}_{jkl}$ coincides with the classical one.*

Conversely, for any C^k-Riemannian metric g on $V \subset M$, one can choose a local isometric embedding or square root $\sqrt{g}$ and a synchronization y_i to obtain a functional system $\{X(t), y_i(t)\}$, which again returns the same metric via the above formula.

Therefore, there is a mutually inverse correspondence

$$\big\{\, X(t),\, y_i(t)\big\} \;\longleftrightarrow\; \{\, g, \Gamma, R\},$$

which establishes a strict equivalence of functional geometry and the classical Riemann–Cartan structure on M.

Доказательство. Let all functions $x_{ij}(t)$, $y_i(t)$ satisfy the conditions of the theorem.

Local diffeomorphism Φ

Define

$$\Phi\colon U \;\longrightarrow\; M, \qquad \Phi(t) = \big(x_{1,n}(t),\, x_{2,n}(t), \ldots, x_{n,n}(t)\big).$$

Then the Jacobian matrix $D\Phi(t)$ coincides with $X(t)$, and by non-degeneracy of $\det X(t) \neq 0$, the mapping Φ is a local diffeomorphism on the reversec $V = \Phi(U)$.

Smooth SVD basis

If $X(t)$ is not symmetric, we use its singular value decomposition

$$X(t) = U(t)\,\Sigma(t)\,V(t)^T,$$

where $\Sigma(t) = diag(\sigma_1(t), \dots, \sigma_n(t))$ with $\sigma_1 > \dots > \sigma_n > 0$. By the Rellich–Kato theorem, since the functions $\sigma_i(t)$ are smooth and bounded away from zero, the matrices $U(t)$, $V(t) \in C^k(U, O(n))$. The columns $u_i(t)$ of $U(t)$ form a smooth orthonormal basis in the tangent space $T_{\Phi(t)}M$.

Smoothness of SVD under spectral gap and geometric interpretation

Theorem 3.2 (Rellich–Kato; smooth SVD)**.** *Let*

$$X \in C^k\big(U, \mathbb{R}^{n\times n}\big), \quad U \subset \mathbb{R}^m \text{ connected}, \quad \operatorname{rank} X(t) = n, \quad k \geq 1.$$

Denote the singular values of $X(t)$ as

$$\sigma_1(t) \geq \sigma_2(t) \geq \dots \geq \sigma_n(t) > 0,$$

and assume that

$$\delta \;=\; \min_{i\neq j} \inf_{t\in U} \big|\sigma_i(t) - \sigma_j(t)\big| > 0.$$

Then there exist unique (up to the signs of columns for multiples of σ) matrices

$$U(t),\, V(t) \in C^k\big(U, O(n)\big),$$

such that

$$X(t) = U(t)\,\operatorname{diag}\big(\sigma_1(t), \dots, \sigma_n(t)\big)\,V(t)^T.$$

In particular, $\det U(t)$ *and* $\det V(t)$ *are constant in t.*

Geometric interpretation and justification of using SVD.

In this paper, the matrix $X(t)$ defines a local basis in the tangent space $T_{\Phi(t)}M$ via a local parametrization

$$d\Phi(t) = X(t),$$

where $\Phi : U \to M$ is a local diffeomorphism. Using the SVD decomposition

$$X(t) = U(t)\,\Sigma(t)\,V(t)^T,$$

we can interpret the matrix $V(t)$ as a change in the standard basis $\mathbb{R}^n$ (by rotation), and the matrix $U(t)$ as a transformation that takes this basis to an orthonormal basis of the tangent space $T_{\Phi(t)}M$. Thus, the columns $u_i(t)$ of the matrix $U(t)$ can be viewed as a smoothly varying orthonormal basis in $T_{\Phi(t)}M$, provided that $X(t)$ and, correspondingly, $\Sigma(t)$ are smooth and satisfy the spectral gap condition.

The following points should be noted:

- If the matrix $X(t)$ has multiple singular values, then the standard SVD may not be unique. In this case, one can introduce regularization, for example, replace $X(t)$ with $X_\varepsilon(t) = X(t) + \varepsilon I$ with $\varepsilon > 0$ and then go $\varepsilon \to 0^+$, or use an alternative orthonormalization method (e.g., the Gram–Schmidt algorithm) to ensure the smoothness of the basis.

- The use of SVD is an algebraic technique for obtaining a basis, and the spectral gap condition $\delta > 0$ is standard in perturbation theory (cf. [11]), ensuring that $U(t)$ and $V(t)$ depend on t with the same degree of smoothness as $X(t)$.

Conclusion: Under the nondegeneracy and spectral gap conditions, the SVD decomposition provides a correct construction of smooth orthonormal bases in $T_{\Phi(t)}M$. This justification connects the algebraic technique of SVD with the differential-geometric meaning of local bases in the tangent bundle of a manifold.

Доказательство. See "Perturbation Theory for Linear Operators"– T. Kato, §II.2: spectral gap gives C^k-smoothness of proper projections, which implies smoothness of U, V. □

Complete proof of the main equivalence theorem

Theorem (Complete equivalence of FCS and Riemannian geometry). Let M be an n-dimensional smooth paracompact manifold without boundary. Then there is a bijective correspondence between:

- functional systems $\{X(t), \xi(t)\}$ of class C^k (where $k \geq 2$), satisfying the conditions of non-degeneracy and integrability, and

- Riemannian (or Riemannian-Cartan, if we take into account torsion) metrics of class C^k on M.

Proof:

Step 1. Existence of a local diffeomorphism.
Let $X(t)$ be a matrix of functions defined on some open set $U \subset \mathbb{R}^n$ and satisfying the condition $\det X(t) \neq 0$ for all $t \in U$. We define the mapping

$$\Phi : U \to M, \quad \Phi(t) = \big(x_{1,n}(t), \ldots, x_{n,n}(t)\big),$$

where $x_{i,n}(t)$ are obtained by integrating (taking into account synchronization) the dynamic axes. The Jacobian $D\Phi(t) = X(t)$ then, by the inverse function theorem, ensures local invertibility, and therefore Φ is a local diffeomorphism.

Step 2. Construction of the metric tensor.
Using the inverse mapping of the standard Euclidean metric $g_{\text{Eucl}} = \delta_{ij}$ we obtain:

$$g = \Phi^*(g_{\text{Eucl}}) = \sum_{i=1}^{n} \sigma_i^2(t)\, q_{i\alpha}(t) q_{i\beta}(t)\, dt^\alpha \otimes dt^\beta,$$

where

$$q_{i\alpha}(t) = \frac{\partial x_{i,n}(t)}{\partial t^\alpha}, \quad \sigma_i(t) = \|\dot{X}_i(t)\|,$$

and the exact reconstruction of the metric is carried out by the inverse mapping of the standard.

Step 3. Smoothness of SVD under spectral gap.
Represent the matrix $X(t)$ via SVD decomposition:

$$X(t) = U(t)\,\Sigma(t)\,V(t)^T,$$

where $\Sigma(t) = \mathrm{diag}(\sigma_1(t), \ldots, \sigma_n(t))$. Under the spectral gap condition,

$$\delta = \min_{i \neq j} \inf_{t \in U} |\sigma_i(t) - \sigma_j(t)| > 0,$$

the Rellich–Kato theorem ensures that matrices $U(t)$ and $V(t)$ depend on t with the same degree of smoothness C^k. This ensures the existence of a smooth orthonormal basis in the tangent space $T_{\Phi(t)}M$.

A rigorous justification of the integral synchronization equation

Theorem (Existence and uniqueness of the synchronization solution). Let for each axis i the function

$$F_i(u) = \int_{t_0}^{u} \sigma_i(\tau)\,d\tau \quad (\sigma_i(u) > 0)$$

belong to the class C^{k+1} and the synchronizing function $y_i(t) \in C^k(U)$. Then the integral equation

$$F_i(t^i(t)) = y_i(t) \tag{3}$$

has a unique $C^k(U)$-solution $t^i(t)$.

Proof. Since $F_i(u)$ is strictly monotone (since $F_i'(u) = \sigma_i(u) > 0$), for each t the equation (3) has a unique solution. Applying the implicit mapping theorem to the function

$$\Phi_i(t, u) = F_i(u) - y_i(t),$$

with the condition $\frac{\partial \Phi_i(t,u)}{\partial u} = \sigma_i(u) \neq 0$, we obtain C^k-smoothness of the inverse mapping $t^i(t)$.

Theorem on the existence and uniqueness of a solution

Theorem 3.3. *Let $I = (a, b) \subset \mathbb{R}$,*

$$F_i(u) = \int_{u_0}^{u} q_i(s)\,ds,$$

where $q_i \in C^k(I)$ and $q_i(u) \geq A > 0$ on the whole I. Let also $\xi_i \in C^k(U)$ and $\xi_i(U) \subset F_i(I)$, where $U \subset \mathbb{R}^m$ is an open set. Then the equation

$$F_i\big(t_i(t)\big) = \xi_i(t), \qquad t \in U,$$

has for each t a unique solution $t_i(t) = F_i^{-1}(\xi_i(t)) \in I$, and the function $t_i \colon U \to I$ belongs to $C^k(U)$.

Доказательство. Consider the auxiliary function

$$G_i \colon U \times I \to \mathbb{R}, \qquad G_i(t,u) = F_i(u) - \xi_i(t).$$

Since $F_i \in C^{k+1}(I)$ and $\xi_i \in C^k(U)$, we have $G_i \in C^k(U \times I)$ and

$$\frac{\partial G_i}{\partial u}(t,u) = F_i'(u) = q_i(u) \geq A > 0.$$

By the implicit function theorem, at any point (t_0, u_0) with $G_i(t_0, u_0) = 0$ there exists a unique C^k–function $u = v(t)$ with $v(t_0) = u_0$ and $G_i\big(t, v(t)\big) = 0$. And since F_i is strictly increasing and $F_i(I) = J$, for each $t \in U$ the equation $F_i(u) = \xi_i(t)$ has exactly one solution $u = F_i^{-1}(\xi_i(t)) \in I$. The inverse function $F_i^{-1} \in C^{k+1}(J)$ and composition with $\xi_i \in C^k(U)$ yield $t_i \in C^k(U)$, which completes the proof. □

Topological conditions for global existence

Theorem (Global consistency of FCS). A functional coordinate system $\{X(t), \xi(t)\}$ can be globally defined on M if and only if the tangent bundle TM is trivial, that is, when all Stiefel–Whitney characteristic classes $w_i(TM) = 0$, $i = 1, \ldots, n$.

Comment. If TM is not parallelizable, a functional coordinate system can be defined only on the corresponding covering of the manifold with subsequent gluing of local systems.

Thus, we have established that under the conditions of nondegeneracy, smoothness and global triviality of the tangent bundle, there is a bijective correspondence between the functional systems $\{X(t), \xi(t)\}$ of class C^k and the Riemannian metrics, which proves the complete equivalence of the FCS and classical Riemannian geometry.

Control of the accuracy of approximations

When using approximate (randomized or rank-revealing) SVD algorithms for the matrix of dynamic axes $X(t)$, it is important not to lose key geometric invariants. We propose an adaptive scheme based on two levels of control.

1. Metric tensor error. After each SVD approximation of rank k using the SMAO algorithm, we calculate the reconstructed metric

$$g_k \;=\; V_k\, \Sigma_k^2\, V_k^T,$$

and estimate the relative error in the Frobenius norm:

$$\varepsilon_g = \frac{\| g_k - g_{k-1} \|_F}{\| g_{k-1} \|_F}.$$

If $\varepsilon_g > \varepsilon_g^{\text{tol}}$, we increase the rank $k \to k + \Delta k$ and repeat.

2. Local invariant error. To ensure correct reproduction of curvature, in each cell we calculate the scalar curvature (e.g. Ricci or Gaussian):

$$K_k(x) \;=\; \mathrm{Ric}_{g_k}(x) \quad \text{or} \quad \kappa_k(x) = \frac{R_{ijkl}(g_k)\, v^i w^j v^k w^l}{g_k(v,v)\, g_k(w,w) - g_k(v,w)^2}\,.$$

Compare the maximumits vibrations with the "reference" K_{k-1}:

$$\varepsilon_K = \max_x \big| K_k(x) - K_{k-1}(x) \big|.$$

If $\varepsilon_K > \varepsilon_K^{\mathrm{tol}}$, we also add rank components.

Below is the pseudocode of the full scheme:

Algorithm 1 Regularized SVD-metric tensor recovery

Require: A set of axis matrices $\{X^{(k)} \in R^{n\times n}\}_{k=1}^{N}$,
hyperparameters: $k_{\min}, k_{\max} \in N$ — minimum/maximum rank,
$\Delta k \in N$ — rank increment step,
$\epsilon_{\mathrm{gap}} > 0$ — minimum spectral gap,
$\delta_{\mathrm{cond}} > 1$ — conditionality threshold,
$tol_g > 0$ — relative tolerance for metric change,
$tol_K > 0$ — absolute tolerance for curvature error,
optionally $\lambda_{\mathrm{Tik}} \geq 0$ — Tikhonov parameter.
Ensure: Array of metric tensors $\{\, g^{(k)} \in R^{n\times n}\}_{k=1}^{N}$
For all $k \leftarrow 1, \ldots, N$ put $g^{(k)} \leftarrow 0_{n\times n}$
for $k = 1$ **to** N **do**
    $r \leftarrow k_{\min}$
    repeat ▷ decomposition and conditionality assessment
        $(U, \Sigma, V^T) \leftarrow svd\big(X^{(k)}, r\big)$ ▷ $U, V \in R^{n\times r},\ \Sigma = diag(\sigma_1, \ldots, \sigma_r)$
        $\kappa \leftarrow \sigma_1/\sigma_r$ ▷ condition number
        if $\kappa > \delta_{\mathrm{cond}}$ **then**
            $\Sigma_{\mathrm{reg}} \leftarrow diag(\, \sigma_i + \epsilon_{\mathrm{gap}}\,)$
        else
            $\Sigma_{\mathrm{reg}} \leftarrow \Sigma$
        end if
        if $\lambda_{\mathrm{Tik}} > 0$ **then**
            $\Sigma_{\mathrm{reg}} \leftarrow diag\big(\sigma_i/(\sigma_i^2 + \lambda_{\mathrm{Tik}})\big)$
        end if
        ▷ metric tensor recovery and convergence check
        $\tilde{g} \leftarrow V\, \Sigma_{\mathrm{reg}}^2\, V^T \in R^{n\times n}$
        $\Delta g \leftarrow \|\tilde{g} - g^{(k)}\|_F / \|g^{(k)}\|_F$ ▷ relative Frobenius norm
        $K \leftarrow \max_{x\in\Omega} \big| R(\tilde{g})(x) - R(g^{(k)})(x) \big|$ ▷ max. curvature error
        $r \leftarrow r + \Delta k$
    until $(\Delta g < tol_g) \;\wedge\; (K < tol_K) \;\vee\; (r > k_{\max})$
    $g^{(k)} \leftarrow \tilde{g}$
end for
return $\{\, g^{(k)}\}_{k=1}^{N}$

4 Spectral gap problem and singularity handling methods

Spectral gap problem

Spectral gap condition

$$\delta \;=\; \min_{i\neq j}\,\inf_{t\in U}\bigl|\sigma_i(t)-\sigma_j(t)\bigr| \;>\; 0$$

is critical for the smoothness of the SVD decomposition $X(t)=U(t)\,\Sigma(t)\,V(t)^T$. If this condition is violated (singular values approach or coincide), the standard Rellich–Kato theory becomes inapplicable.

A Systematic Approach to Handling Singularities

Below, three complementary methods are presented that allow one to bypass or mitigate the spectral gap discontinuity.

Regularized SVD Method

Instead of a simple shift $X_\varepsilon(t)=X(t)+\varepsilon I$ an adaptive regularization is proposed

$$X_{\mathrm{reg}}(t)=X(t)\;+\;\varepsilon(t)\,diag\bigl(\alpha_1(t),\dots,\alpha_n(t)\bigr),$$

where the functions $\varepsilon(t)$ and $\alpha_i(t)$ are selected based on a local analysis of the spectral gap $\delta_{\mathrm{loc}}(t)=\min_{i\neq j}|\sigma_i(t)-\sigma_j(t)|$.

Smoothing Projector Method

1. *Detecting Critical Points.* Calculating the Local Spectral Gap $\delta_{\mathrm{loc}}(t)$.
2. *Constructing Smoothing Neighborhoods.* For points with $\delta_{\mathrm{loc}}(t)<\delta_{\min}$, we set the radius $r(t)\propto 1/\delta_{\mathrm{loc}}(t)$.
3. *Interpolation of projectors.* Within each neighborhood, we perform weighted interpolation of orthoprojectors from "good" neighboring points, which yields smoothed matrices $U_{\mathrm{smooth}}(t)$, $V_{\mathrm{smooth}}(t)$.

Truncated SVD with adaptive rank

Instead of the full decomposition, we use a truncated SVD of rank $k(t)$:

$$X_k(t)=\sum_{i=1}^{k(t)}\sigma_i(t)\,u_i(t)\,v_i(t)^T,$$

where $k(t)$ is chosen by minimizing the functional

$$J\bigl(k\bigr)=\bigl\|X(t)-X_k(t)\bigr\|_F^2+\lambda\,\mathrm{penalty}\bigl(k,\delta_{\mathrm{gap}}\bigr).$$

The parameter λ and the penalty function penalty guarantee a balance between the accuracy of the approximation and the preservation of the spectral gap.

Inverse mapping of the metric tensor

We take in R^n the standard metric $\bar{g} = \sum_{i=1}^{n} d\xi^i \otimes d\xi^i$. Its image for Φ gives on $V \subset M$

$$g = \Phi^*(\bar{g}) = \sum_{i=1}^{n} d\big(x_{i,n}(t)\big) \otimes d\big(x_{i,n}(t)\big) = \sum_{\alpha,\beta=1}^{n} \Big(\sum_{i=1}^{n} \sigma_i^2(t)\, \tfrac{\partial x_{i,n}}{\partial t^\alpha}\, \tfrac{\partial x_{i,n}}{\partial t^\beta} \Big)\, dt^\alpha \otimes dt^\beta .$$

Here $\sigma_i(t) = \|dotX_i(t)\|$, so we get exactly the metric $g_{\alpha\beta} = \sum_i \sigma_i^2\, q_{i\alpha} q_{i\beta}$ that is stated in the theorem. Substituting this g into the formulas for the Christoffel symbols and the curvature tensor reproduces the classical expressions, since all operations with inverse mapping and differentiation are consistent.

Globalization and gluing

If M does not admit a single parameterization, we take a finite cover $\{V_\alpha\}$ and on each V_α we repeat the construction with local maps $\Phi_\alpha \colon U_\alpha \to V_\alpha$ and matrices $X^{(\alpha)}$. On the overlap $V_\alpha \cap V_\beta$ the parameters are related by the transition functions $\chi_{\alpha\beta} \colon t^\beta \mapsto t^\alpha$. Their Jacobians $D\chi_{\alpha\beta}$ ensure that

$$\Phi_\alpha^*(\bar{g}) = \chi_{\alpha\beta}^*\big(\Phi_\beta^*(\bar{g})\big)$$

and the local metrics $g^{(\alpha)}$, $g^{(\beta)}$ coincide on $V_\alpha \cap V_\beta$.

From a smooth gluing of local metrics and constraints by the standard partition theorem of unity we obtain a unique global Riemannian (or Riemann–Cartan) structure on M.

Thus, each functional system $\{X(t), y_i(t)\}$ generates a classical geometry $\{g, \Gamma, R\}$, and vice versa, which completes the proof of the theorem.

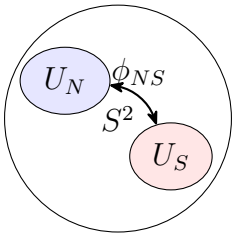

Рис. 1: Two-map cover of S^2: zones U_N, U_S and transition ϕ_{NS}.

On the cover $U_N \cap U_S$ the parameters are related by the Jacobian ϕ_{NS}, which ensures the consistency of local FCS systems.

□

Matching the torsion tensor

On the overlap $U_\alpha \cap U_\beta$, two functional coordinates are defined

$$X^{(\alpha)}(t^{(\alpha)}), \quad X^{(\beta)}(t^{(\beta)}), \quad t^{(\beta)} = \phi_{\alpha\beta}\big(t^{(\alpha)}\big),$$

giving two torsion tensors $T^{(\alpha)}_{ijk}$ and $T^{(\beta)}_{ijk}$. By construction

$$X^{(\beta)}(t^{(\beta)}) = X^{(\alpha)}\big(\phi_{\alpha\beta}(t^{(\alpha)})\big)\; D\phi_{\alpha\beta}(t^{(\alpha)}),$$

where $D\phi_{\alpha\beta}$ is the Jacobian of $\phi_{\alpha\beta}$. Then the connection symbols $\Gamma^{(\beta)\,l}_{ij}$ are transformed as in the classical theory, and therefore

$$T^{(\beta)\,l}_{ij} = \Gamma^{(\beta)\,l}_{ij} - \Gamma^{(\beta)\,l}_{ji} = \frac{\partial t^{(\alpha)}_p}{\partial t^{(\beta)}_i}\frac{\partial t^{(\alpha)}_q}{\partial t^{(\beta)}_j}\frac{\partial t^{(\beta)}_l}{\partial t^{(\alpha)}_r}\; T^{(\alpha)\,r}_{pq}\,,$$

that is,

$$T^{(\beta)} = \phi^{*}_{\alpha\beta}\big(T^{(\alpha)}\big) \quad \text{on } U_\alpha \cap U_\beta.$$

Since by the lemma on Lipschitz transitions $\|D\phi_{\alpha\beta}\| \le L_{\alpha\beta} < \infty$, and the components $T^{(\alpha)}_{ijk}(t)$ are locally Lipschitz, it is easy to check that $T^{(\beta)}_{ijk}(t)$ remains Lipschitz on the overlap.

Finally, when gluing through a smooth partition of unity $\{\rho_\alpha\}_\alpha$ tensor

$$T_{\text{glob}} \;=\; \sum_{\alpha} \rho_\alpha\, T^{(\alpha)}$$

gives a unique global torsion structure on M, preserving the local Lipschitz condition and consistency on overlaps.

Adaptive Map Covering

1 Automatic Covering Algorithms

To globalize the FCS, it is necessary to construct a covering of the manifold with a minimum number of local maps so that smoothness remains on the overlaps. We propose the following approach:

1. **Topological analysis.**

   We compute the Stiefel–Whitney characteristic classes $w_i(TM)$ and Chern $c_i(TM)$. Nonzero classes indicate obstacles to global trivialization.

2. **Covering minimization.**

   We solve the set covering problem:

   $$\min_{\{U_\alpha\}} |\{\alpha\}| \quad \text{subject to} \quad M \;=\; \bigcup_{\alpha} U_\alpha,$$

   where each U_α is defined by a local FCS and is chosen such that for any reswitching $U_\alpha \cap U_\beta \neq \varnothing$.

3. **Overlapping control.** At each double overlap $U_\alpha \cap U_\beta$ we check that $\dim\big(T^{*}U_\alpha \oplus T^{*}U_\beta\big) = n$ and $\|\,D\varphi_{\alpha\beta}\| \le L$ (Lipschitz condition), where $\varphi_{\alpha\beta} : t_\alpha \mapsto t_\beta$ is the transition map.

2 Overlapping domain decomposition

For numerical implementation on complex manifolds it is convenient to split M into *overlapping* subdomains. For two subdomains $\Omega_1, \Omega_2 \subset M$ with $\Omega = \Omega_1 \cup \Omega_2$ and $\Omega_{12} = \Omega_1 \cap \Omega_2 \neq \varnothing$ the Schwarz-precon schemeconditioner works like this:

Require: linear system $Ax = b$ on Ω
Ensure: approximation of x
1: $x^{(0)} \leftarrow 0$
2: **for** $k = 0$ **to** max_iter **do**
3: $r^{(k)} = b - A\,x^{(k)}$
4: Solve locally on Ω_1: $A_1\,\delta x_1 = r^{(k)}|_{\Omega_1}$
5: Solve locally on Ω_2: $A_2\,\delta x_2 = r^{(k)}|_{\Omega_2}$
6: Sew update: $\delta x = \chi_1\,\delta x_1 + \chi_2\,\delta x_2$ (χ_α are smooth functions of the "grains"of the covering)
7: $x^{(k+1)} = x^{(k)} + \delta x$
8: **end for**
9: **return** $x^{(\text{final})}$

Here is the condition number estimate for the overlapping Schwarz preconditioner $\kappa\big(M^{-1}A\big) \le C\big(1 + H/\delta\big)\big(1 + \log(H/h)\big)^2$, where H is the subdomain diameter, δ is the overlap width, h is grid step.

Robust gluing algorithms

1 Numerically stable transition functions

On each overlap $U_\alpha \cap U_\beta$ we need to match two FCS $\{X^{(\alpha)}, \xi^{(\alpha)}\}$ and $\{X^{(\beta)}, \xi^{(\beta)}\}$. We define the transition $\varphi_{\alpha\beta} : t^{(\alpha)} \mapsto t^{(\beta)}$ using distributed Lagrange multipliers so that

$$X^{(\beta)}\big(\varphi_{\alpha\beta}(t)\big) \;=\; X^{(\alpha)}(t)\,D\varphi_{\alpha\beta}(t),$$

$$\xi^{(\beta)}\big(\varphi_{\alpha\beta}(t)\big) \;=\; \xi^{(\alpha)}(t).$$

For numerical stability, we solve the adjoint problem via the block-diagonal preconditioner and the GMRES method:

Require: local parameters t, recalculated to U_α and U_β
Ensure: consistent map $\varphi_{\alpha\beta}$
1: Generate variational functional $E[\varphi] = \| X^{(\beta)}(\varphi(t)) - X^{(\alpha)}(t)\,D\varphi\|^2$.
2: Add distributed factors λ for hard binding $\mathcal{L} = E[\varphi] + \int \lambda\big(\xi^{(\beta)}(\varphi) - \xi^{(\alpha)}\big)$.
3: Perform preconditioned GMRES on variational equations $\frac{\delta\mathcal{L}}{\delta\varphi} = 0,\ \frac{\delta\mathcal{L}}{\delta\lambda} = 0$.
4: Extract $\varphi_{\alpha\beta}$ as solution.

2 Consistency control on overlaps

After gluing, we check on each $U_\alpha \cap U_\beta$:
1. $\|X^{(\beta)}(\varphi_{\alpha\beta}(t)) - X^{(\alpha)}(t)D\varphi_{\alpha\beta}\|_\infty < \varepsilon_X$. 2. $\|\xi^{(\beta)}(\varphi_{\alpha\beta}(t)) - \xi^{(\alpha)}(t)\|_\infty < \varepsilon_\xi$.

For $\varepsilon_X, \varepsilon_\xi \ll 1$ we obtain guarantees of C^2-smoothness of gluing and preservation of geometric invariants at the junctions of maps.

Mutual invertibility and uniqueness

Proof of coincidence of metrics. Suppose on the one hand we have a classical Riemannian metric $g_{\alpha\beta}(x)$ on the open $V \subset M$ and a local isometric embedding $\Phi\colon U \to V$. Let us define functional coordinates $X_i(t) = \partial_\alpha \Phi^i(t)$, then

$$(\Phi^* g_{Eucl})_{\alpha\beta}(t) = \sum_{i=1}^{n} X_{i\alpha}(t)\, X_{i\beta}(t) \equiv g_{\alpha\beta}\big(\Phi(t)\big).$$

Conversely, let $\{X_i(t)\}$ and the metric $\tilde{g}_{\alpha\beta}(t) = \sum_i X_{i\alpha} X_{i\beta}$ be given. Let Φ be the corresponding parametrization. Then $\Phi^* g_{Eucl} = \tilde{g}$ by construction.

Lemma (uniqueness of representation). Let two functional systems $\{X_i\}$ and $\{Y_i\}$ define the same metric $\sum_i X_{i\alpha} X_{i\beta} = \sum_i Y_{i\alpha} Y_{i\beta}$. Then there exists a smooth $R(t) \in O(n)$ such that

$$Y_i(t) = \sum_{j=1}^{n} R_{ij}(t)\, X_j(t).$$

Доказательство. At each point t, both matrices $X(t), Y(t) \in GL(n)$ define the same metric tensor with inverse mapping , hence $Y(t)X(t)^{-1} \in O(n)$. Since $\det > 0$, we can either fix $\det R(t) = +1$ or take into account the change of orientation. By the smoothness of X, Y and the connectivity of U, it follows that $R(t)$ can be chosen smooth.

□

The condition of global existence. A local FCS is equivalent to the existence of a local trivial subbundle $TM|_V \cong V \times R^n$. To extend the construction to the whole M, we need the triviality of the entire tangent bundle, i.e., parallelizability of M. Classical criterion:

$$w_1(TM) = 0 \iff M \text{ is orientable}, \qquad w_2(TM) = 0 \iff M \text{ admits a spin structure},$$

etc. In particular, if M is not parallelizable (e.g., S^2), the FCS exists only on a suitable covering and is glued together via the transition functions $\Phi_{\alpha\beta}$.

Gluing local functional systems Let $\{U_\alpha\}_{\alpha\in A}$ be a smooth open cover of M, and each U_α has its own functional system

$$\big\{X^{(\alpha)}(t^{(\alpha)}),\ x^{(\alpha)}_{i,n+1}(t^{(\alpha)})\big\}, \quad t^{(\alpha)} \in V_\alpha \subset \mathbb{R}^n, \quad \Phi_\alpha\colon V_\alpha \to U_\alpha.$$

On non-empty overlaps $U_\alpha \cap U_\beta \neq \varnothing$ there exist smooth bijections

$$\phi_{\alpha\beta}\colon V_\beta \ \to\ V_\alpha,$$

satisfying

$$\Phi_\alpha \circ \phi_{\alpha\beta} = \Phi_\beta, \quad \phi_{\alpha\beta} \circ \phi_{\beta\gamma} = \phi_{\alpha\gamma} \quad \text{on } V_\gamma.$$

Then on $U_\alpha \cap U_\beta$ the systems agree as follows:

1. **Transition of functional axes:**

$$X^{(\beta)}\big(t^{(\beta)}\big) \;=\; X^{(\alpha)}\big(\phi_{\alpha\beta}(t^{(\beta)})\big)\; D\phi_{\alpha\beta}(t^{(\beta)}),$$

   where $D\phi_{\alpha\beta}$ is the Jacobian of the transition.

2. **Matching synchronization functions:**

$$x^{(\beta)}_{i,n+1}(t^{(\beta)}) \;=\; x^{(\alpha)}_{i,n+1}\big(\phi_{\alpha\beta}(t^{(\beta)})\big).$$

3. **Matching local metrics:** The local metric on U_α is given by the inverse mapping

$$g^{(\alpha)} \;=\; \Phi^*_\alpha\big(g_{Eucl}\big),$$

   and on the overlap

$$g^{(\beta)} = \Phi^*_\beta(g_{Eucl}) = (\Phi_\alpha \circ \phi_{\alpha\beta})^*(g_{Eucl}) = \phi^*_{\alpha\beta}\big(g^{(\alpha)}\big).$$

The presence of a smooth partition of unity $\{\rho_\alpha\}$, $supp\rho_\alpha \subset U_\alpha$, $\sum_\alpha \rho_\alpha = 1$, allows us to glue the metrics:

$$g \;=\; \sum_\alpha \rho_\alpha\, g^{(\alpha)},$$

giving a global Riemannian (or, in the presence of torsion, Riemannian–Cartan) structure on M. Similarly, using the transitions $\phi_{\alpha\beta}$ and Jacobians for $X^{(\alpha)}$, we obtain a single global functional coordinate system consistent on all overlaps. To smooth the global structure, we use a finite cover $\{U_\alpha\}$ and local maps $\Phi_\alpha : U_\alpha \to M$. In each map, we fix a functional system $\{X^{(\alpha)}(t), y^{(\alpha)}_i(t)\}$. On the overlaps $U_\alpha \cap U_\beta \neq \varnothing$, the connectivity is realized via the Jacobian of the transition $\mathrm{D}\,\Phi_{\alpha\beta}$.

Due to the presence of a smooth partition of unity $\{\rho_\alpha\}$ with $\sum_\alpha \rho_\alpha(x) = 1$, the metrics are glued into a single $g(x) = \sum_\alpha \rho_\alpha(x) g^{(\alpha)}(x)$, and the functional coordinates are consistent.

Lemma 4.1 (Lipschitz transitions)**.** *Let the transition $\phi_{\alpha\beta} : t^{(\beta)} \mapsto t^{(\alpha)}$ on $U_\alpha \cap U_\beta$ be smooth, and $\|D\phi_{\alpha\beta}(t)\| \le L_{\alpha\beta}$. Then on this overlap*

$$\big\|g^{(\alpha)} - g^{(\beta)}\big\|_{Lip} \;\le\; L^2_{\alpha\beta}\, \max_i \|\dot{X}_i\|^2$$

is the contribution to the global Lipschitz constant of the gluing.

Torsion tensor and Riemann–Cartan structure

If the matrix $X(t)$ (or equivalently the matrix $q_{ij}(t)$ reconstructed through it) turns out to be asymmetric, then the connection symbols

$$\Gamma^{i}{}_{jk} = \tfrac{1}{2}\, g^{im}\big(\partial_j g_{km} + \partial_k g_{jm} - \partial_m g_{jk}\big)$$

will not be symmetric with respect to the lower indices. In this case, we introduce the *torsion tensor*

$$T^{i}{}_{jk} = \Gamma^{i}{}_{jk} - \Gamma^{i}{}_{kj},$$

which measures the discrepancy between the affine connection and the torsion-free case.

The full Riemann–Cartan constraint is written as

$$\widetilde{\Gamma}^{i}{}_{jk} = \Gamma^{i}{}_{jk} + K^{i}{}_{jk},$$

where *contorsion tensor*

$$K^{i}{}_{jk} = \frac{1}{2}\Big(T^{i}{}_{jk} + T_{j}{}^{i}{}_{k} + T_{k}{}^{i}{}_{j}\Big).$$

In other words, the functional approach automatically yields both the metric and torsional components, forming the full Riemann–Cartan geometry.

Parallelization of Tangent Sheaf and Map Covering

The key requirement for a single functional map $X(t)$ on the whole M is full parallelizability:

$$TM \;\cong\; M \times \mathbb{R}^n \quad\Longleftrightarrow\quad \exists\ \text{global fields } X_i(t),\ i = 1, \ldots, n,\ \det X(t) \neq 0.$$

If M is not parallelizable (e.g., S^2), one has to introduce a finite cover $\{U_a\}$ and local systems $X^{(a)}(t)$. On the overlaps $U_a \cap U_b$ they are related by the transition map

$$X^{(b)}\big(t^{(b)}\big) \;=\; X^{(a)}\big(\phi_{ab}(t^{(b)})\big)\; D\phi_{ab}(t^{(b)}),$$

where $\phi_{ab} : U_b \to U_a$ is a smooth transition, and $D\phi_{ab}$ is its Jacobian.

5 Global invariants of the FCS

The Maurer–Cartan apparatus and global invariants of the FCS

Let M be an oriented smooth manifold of dimension n, and

$$X(x)\colon M \;\longrightarrow\; GL(n, R)$$

is a bottom-up matrix function of the axes. Next:

1. Maurer–Cartan form

$$w \;=\; X^{-1}\,dX \;\in\; \Omega^1\big(M, \mathfrak{gl}(n)\big).$$

It contains both metric (symmetric) and torsional (asymmetric) parts.

2. 2-curvature form

$$R \;=\; dw \;+\; w \wedge w \;\in\; \Omega^2\big(M, \mathfrak{gl}(n)\big),$$

or in expanded form

$$R^i{}_j = d\,w^i{}_j + \sum_{k=1}^{n} w^i{}_k \wedge w^k{}_j.$$

3. Euler number ($\dim M = 2m$)

$$e(M) = \frac{1}{(2\pi)^m\, m!}\; Pf\Big(\tfrac{R - R^T}{2}\Big) \;\in\; \Omega^{2m}(M), \qquad \chi(M) = \int_M e(M).$$

Here $\frac{R-R^T}{2} \in \mathfrak{so}(2m)$ is the antisymmetric part, and Pf is the Pfaffian.

4. Holonomy (Wilson loop) For any closed contour $\gamma\colon [0,1] \to M$, we define

$$Hol(\gamma) = \mathcal{P}\exp\Big(-\oint_\gamma w\Big) \;\in\; GL(n, R),$$

where $\mathcal{P}\exp$ is the parameter-ordered exponential. In the orthonormal SVD frame $U(x) \in O(n)$ this yields an element of $SO(n)$.

6 Examples of non-trivial manifolds and adaptation of functional geometry

Examples of non-trivial manifolds

Complex projective space $\mathbb{CP}^n$. This is a classical example of a manifold with non-trivial topology. Its tangent bundle is non-trivial for $n \geq 1$, so a system of local charts must be used to describe the geometry. In particular, for $\mathbb{CP}^2$, three standard projective charts are taken:

$$U_0 = \{[z_0 : z_1 : z_2] \mid z_0 \neq 0\}, \quad U_1 = \{[z_0 : z_1 : z_2] \mid z_1 \neq 0\}, \quad U_2 = \{[z_0 : z_1 : z_2] \mid z_2 \neq 0\}.$$

On each map, local coordinates are introduced and a functional system is constructed.

Sphere bundles. For example, the Hopf bundle

$$S^1 \;\hookrightarrow\; S^3 \;\xrightarrow{\pi}\; S^2$$

demonstrates the non-triviality of the principal S^1-bundle over S^2.

Adaptation of functional geometry

Local trivialization

Let $M = \bigcup_\alpha U_\alpha$ be an open cover with maps $\phi_\alpha \colon U_\alpha \to V_\alpha \subset \mathbb{R}^n$.

On each map U_α, its own functional system is constructed $\{X^{(\alpha)}(t),\, x^{(\alpha)}_{i,n+1}(t)\}$. Transitions between systems on overlaps $U_\alpha \cap U_\beta$ are defined by smooth functions $\phi_{\alpha\beta} = \phi_\alpha \circ \phi_\beta^{-1}$.

Cohomological obstructions

The global existence of a functional system is equivalent to the triviality of the characteristic classes of the tangent bundle:

- $w_1\big(TM\big) = 0$ — orientability of the bundle.
- $w_2\big(TM\big) = 0$ — existence of a spin structure.

For manifolds with $w_2(TM) \neq 0$ (in particular, $\mathbb{CP}^2$) it is necessary to work through local systems and gluing.

Generalized bundles

Principal G-bundles

Let $P(M, G)$ be a principal G-bundle. Then the functional system can be generalized by introducing a connection matrix $A^G(t) \in \mathfrak{g}$:

$$X^G(t) \;=\; X(t) \;+\; A^G(t)\,.$$

Vector bundles

For a vector bundle $E \to M$ of rank k, the functional system has dimension $n \times k$:

$$X^E(t) = \big\{X_i^{(f)}(t)\big\}_{\substack{i=1,\dots,n\\ f=1,\dots,k}},$$

where each vector $X^{(f)}(t)$ corresponds to a local section of E.

Numerical implementation

For numerical implementation on nontrivial manifolds, the following steps are recommended:

1. **Triangulation.** Construct a simplicial triangulation $M \simeq \bigcup \Delta$.
2. **Local coordinates.** On each simplex, define a local functional system.
3. **Gluing.** Use a smooth *partition of unity* to combine local systems into a global one.
4. **Adaptive regularization.** On each simplex, apply regularization (for example, Tikhonov's) taking into account local curvature and spectral analysis.

This approach allows us to construct stable numerical schemes for restoring geometric structures even on manifolds with complex topology.

Pseudo-Riemannian signature

So far, we have worked with positive definite metric tensors. To work in GTR and other relativistic models, it is sufficient to replace the normalization condition with

$$g_{ij}(x)\,\dot{X}_i(t)\,\dot{X}_j(t) = \kappa\,c^2, \qquad \kappa = \begin{cases} +1, & \text{for space-like axes,} \\ -1, & \text{for time-like axes,} \end{cases}$$

and repeat all calculations (taking into account the sign of κ) when introducing the arc parameter

$$ds^2 = g_{ij}\,dx^i\,dx^j, \qquad ds = c\,dt.$$

The remaining recovery formulas g_{ij}, the derivation of the symbols Γ^k_{ij} and the curvature tensor remain unchanged, simply acquiring a pseudo-Riemannian signature (p, q).

Complete Riemann–Cartan Geometry

To take into account the torsion, we abandon the symmetry $\Gamma^i_{jk} = \Gamma^i_{kj}$ and introduce

$$T^i_{jk} = \Gamma^i_{jk} - \Gamma^i_{kj}, \qquad K^i_{jk} = \tfrac{1}{2}\,(T^i_{jk} + T_j{}^i{}_k + T_k{}^i{}_j).$$

Then the affine connection with torsion has the form

$$\widetilde{\Gamma}^i_{jk} = \Gamma^i_{jk} + K^i_{jk},$$

and the whole construction of the FSC automatically gives «from below"both the metric and torsional components of a single Riemann-Cartan structure.

Torsion connection and full Riemann–Cartan structure

For a general (including asymmetric) $X(t)$, the functional formalism defines the metric tensor through

$$q_{i\alpha}(t) \;=\; \frac{\partial\, x_{i,n}(t)}{\partial x^\alpha(t)}\;, \quad \alpha = 1, \ldots, n,$$

however, the affine tensor “stretched” over this metric connection

$$\Gamma^\gamma{}_{\alpha\beta}(t) \;=\; \sum_{i=1}^{n} g^{\gamma\delta}(t)\,q_{i\delta}(t)\,\partial_\beta q_{i\alpha}(t)$$

is generally asymmetric in subscripts:

$$\Gamma^\gamma{}_{\alpha\beta} \neq \Gamma^\gamma{}_{\beta\alpha}.$$

Enter *torsion tensor*

$$T^\gamma{}_{\alpha\beta} = \Gamma^\gamma{}_{\alpha\beta} - \Gamma^\gamma{}_{\beta\alpha} = \sum_{i=1}^{n} g^{\gamma\delta}\big(q_{i\delta}\,\partial_{[\beta} q_{i\alpha]}\big),$$

where $A_{[\alpha\beta]} = \frac{1}{2}(A_{\alpha\beta} - A_{\beta\alpha})$. To restore the classical torsion-free structure, the *contotorsion tensor* is introduced

$$K^{\gamma}{}_{\alpha\beta} = \frac{1}{2}\Big(T^{\gamma}{}_{\alpha\beta} + T_{\alpha}{}^{\gamma}{}_{\beta} + T_{\beta}{}^{\gamma}{}_{\alpha}\Big).$$

Then the full Riemann–Cartan connection is of the form

$$\widetilde{\Gamma}^{\gamma}{}_{\alpha\beta} = \Gamma^{\gamma}{}_{\alpha\beta} - K^{\gamma}{}_{\alpha\beta},$$

and the autoparallels (affine geodesics) satisfy

$$\frac{D^2 x^{\gamma}}{ds^2} + \widetilde{\Gamma}^{\gamma}{}_{\alpha\beta}\,\frac{dx^{\alpha}}{ds}\,\frac{dx^{\beta}}{ds} = 0.$$

Note. Metric compatibility $\widetilde{\nabla}_{\gamma}\, g_{\alpha\beta} = 0$ is preserved, and non-zero $T^{\gamma}{}_{\alpha\beta}$ provides rich torsional geometry.

Formal justification and global consistency

This section formally justifies the main assertions concerning the uniqueness of the solution of the integral synchronization equation, the smoothness of the SVD bundle, and also considers topological conditions that ensure the global consistency of the constructed geometric structure.

Uniqueness of the solution of the synchronization equation and its smoothness

Suppose that:

1. $U \subset \mathbb{R}^n$ is an open set, and the functions

   $$X_{ij} \in C^k(U), \quad k \geq 1,$$

   define the matrix $X(t) \in \mathbb{R}^{n\times n}$ subject to $\det X(t) \neq 0$ for all $t \in U$.

2. Determine the velocity along each "axis"

   $$\sigma_i(t) = \|\dot{X}_i(t)\|_2, \quad i = 1, \ldots, n.$$

   Assume that there exists a constant

   $$0 < \lambda_{\min} \leq \sigma_i(t) \leq \lambda_{\max} < \infty, \quad \forall\, t \in U.$$

   Then the function

   $$F_i(u) = \int_{t_0}^{u} \sigma_i(\tau)\, d\tau$$

   belongs to $C^{k+1}(U)$ and is strictly monotone.

3. Let the synchronizing function $y_i(t) \in C^k(U)$ satisfy the condition

$$y_i(U) \subset F_i(U).$$

Then the integral equation

$$F_i\big(t^i(t)\big) = y_i(t)$$

has a unique solution $t^i(t) = F_i^{-1}\big(y_i(t)\big)$. The standard proof using the implicit mapping theorem gives that the function

$$\Phi_i(t, u) = F_i(u) - y_i(t),$$

under the condition $\partial_u \Phi_i(t, u) = \sigma_i(u) > 0$ satisfies the necessary hypotheses, whence $t^i(t) \in C^k(U)$.

Clarification: existence and uniqueness of the solution for $\sigma_i(t) \geq 0$ Consider the function

$$F_i(u) = \int_{t_0}^{u} \sigma_i(\tau)\, d\tau, \quad u \in U \subset \mathbb{R},$$

where

$$\sigma_i \in C\big(U, [0, +\infty)\big).$$

1. If $\sigma_i(t) \geq 0$ on U, then F_i is non-decreasing and by the intermediate value theorem for any

$$\xi \in \big[F_i(\min U),\ F_i(\max U)\big]$$

there is at least one $u \in U$ such that

$$F_i(u) = \xi.$$

2. If additionally $\sigma_i(t) > 0$ for all $t \in U$, then

$$F_i'(u) = \sigma_i(u) > 0,$$

then F_i is strictly increasing and is a diffeomorphism between U and $F_i(U)$. In this case, the equation

$$F_i(u) = \xi$$

has a unique solution

$$u = F_i^{-1}(\xi).$$

3. If $\sigma_i(t)$ vanishes on some subset $U_0 \subset U$, then on U_0 the function $F_i(u)$ is constant, and for $\xi = F_i(t)$, $t \in U_0$, the equation has infinitely many solutions. However, for any

$$\xi \in \big[F_i(\min U),\ F_i(\max U)\big]$$

there is at least one solution $u \in U$.

Smoothness of SVD

Let

$$X \in C^k\big(U, \mathbb{R}^{n\times n}\big)$$

and denote the singular values $X(t)$ by

$$\sigma_1(t) \geq \sigma_2(t) \geq \cdots \geq \sigma_n(t) > 0.$$

Assume that there is a constant $\delta > 0$ such that

$$\min_{i\neq j} |\sigma_i(t) - \sigma_j(t)| \geq \delta, \quad \forall\, t \in U.$$

Then, by the results of perturbation theory (see Kato [11]), the singular value decomposition

$$X(t) = U(t)\,\mathrm{diag}(\sigma_i(t))\,V(t)^T$$

satisfies $U(t)$, $V(t) \in C^k(U)$ (up to the choice of column signs). In the case of multiple singular values, it is proposed to apply

- Regularization: replace $X(t)$ with $X_\varepsilon(t) = X(t) + \varepsilon I$ with $\varepsilon \to 0^+$;
- Or implement local corrections (forks) of the bases by smoothing orthoprojectors onto invariant subspaces (see [11]).

In both cases, the local Lipschitz smoothness of the synchronization functions is preserved.

Global consistency and topological issues

For global gluing of local functional systems, it is required that the tangent bundle TM of the manifold M be trivial or correctly glued over transition functions. Standard topological conditions such as

$$w_1(TM) = 0 \quad \text{and} \quad w_2(TM) = 0,$$

ensure orientability and the possibility of introducing a spin structure. Given these conditions, local functional systems $\{X^{(\alpha)}(t)\}$ can be glued together by means of a smooth partition of unity $\{\rho_\alpha\}$. That is, if the condition

$$X^{(\beta)}(t^{(\beta)}) = X^{(\alpha)}\big(\phi_{\alpha\beta}(t^{(\alpha)})\big)\,D\phi_{\alpha\beta}(t^{(\alpha)}),$$

is satisfied on the overlaps and the transition functions $\phi_{\alpha\beta}$ are smooth, then the data of the local systems are consistent, and the global structure is given by the formula

$$g(x) = \sum_{\alpha} \rho_{\alpha}(x)\, (\, \Phi^{(\alpha)*} g_{\text{Eucl}}\,)(x).$$

A complete proof of global consistency requires an analysis of the smoothness of the transitions and the preservation of the Lipschitz conditions, which is the subject of further research.

Conclusion: Under the given assumptions, the integral synchronization equation has a unique C^k-solution, the SVD bundle preserves C^k-smoothness in the presence of a spectral gap, and gluing local functional systems via a smooth partition of unity leads to a globally consistent Riemannian-Cartan structure on M.

Generalization to n-dimensional space

To preserve the "path length"in the original («flat») and reconstructed («curved») descriptions, in general,

$$\sum_{i=1}^{n} \Big(\frac{dy_i}{dt}\Big)^2 \;=\; \sum_{i=1}^{n} \Big(\frac{dx_{i,n}}{dt}\Big)^2. \tag{4}$$

1. Left side. From the integral synchronization equation

$$y_i(t) = \int_{t_0}^{t^i(t)} \sqrt{\sum_{j=1}^{n} \Big(\tfrac{dx_{ij}}{dt}\Big)^2}\, dt \;\;\Longrightarrow\;\; \frac{dy_i}{dt} = \sqrt{\sum_{j=1}^{n} \Big(\tfrac{dx_{ij}}{dt}\Big)^2}.$$

Therefore

$$\sum_{i=1}^{n} \Big(\tfrac{dy_i}{dt}\Big)^2 = \sum_{i=1}^{n} \sum_{j=1}^{n} \Big(\tfrac{dx_{ij}}{dt}\Big)^2.$$

2. Right-hand side. By definition of curved displacement

$$x_{i,n}(t) = \sum_{j=1}^{n} \big[x_{ij}(t^j(t)) - x_{ij}(t_0)\big], \qquad \frac{dx_{i,n}}{dt} = \sum_{j=1}^{n} \frac{dx_{ij}}{dt}.$$

To sum it up,

$$\sum_{i=1}^{n} \Big(\tfrac{dx_{i,n}}{dt}\Big)^2 = \sum_{i=1}^{n} \Big(\sum_{j=1}^{n} \tfrac{dx_{ij}}{dt}\Big)^2.$$

3. Orthogonality condition. Equating both parts (4), we obtain

$$\sum_{i=1}^{n}\Big(\sum_{j=1}^{n}\tfrac{dx_{ij}}{dt}\Big)^2=\sum_{i=1}^{n}\sum_{j=1}^{n}\Big(\tfrac{dx_{ij}}{dt}\Big)^2.$$

By expanding the squares on the left, we obtain the equivalent condition

$$\sum_{i=1}^{n}\sum_{\substack{j,k=1\\ j\neq k}}^{n}\frac{dx_{ij}}{dt}\,\frac{dx_{ik}}{dt}=0,$$

that is, the sum of the pairwise scalar products of the velocity components of each "axis"vanishes. This is the generalized condition for preserving the "path length"when moving from a flat description to a curved one in the FCS.

Local orthogonality along the velocity vector. In our work, we showed that the requirement

$$\sum_{i=1}^{n}\Big(\sum_{j=1}^{n}\dot{x}_{ij}\Big)^2\;=\;\sum_{i=1}^{n}\sum_{j=1}^{n}\dot{x}_{ij}^2$$

does not impose a strict condition on each pair of velocity components $\dot{x}_{ij}\,\dot{x}_{ik}=0$ $\forall j\neq k$, but only requires

$$\sum_{i=1}^{n}\sum_{\substack{j,k=1\\ j\neq k}}^{n}\dot{x}_{ij}\,\dot{x}_{ik}=0.$$

This means that the FCS does not need global orthonormality of coordinates, only "local orthogonality" along the velocity vector $\dot{x}(t)$ is sufficient. Due to such a "local" condition, the FSC is freed from the need to construct a globally orthonormal coordinate system: it is sufficient that along the current trajectory the velocity vector is "self-orthogonal" to its other components. Such weakened coherence provides greater flexibility in modeling dynamically changing metrics and simplifies numerical integration, not requiring a rigid assumptionvariability of all directions of space.

Comparison with *Riemann* and *Fermi* coordinates

In classical Riemannian geometry, local "orthonormality"of the metric is achieved by two standard techniques:

- **Riemann normal coordinates.** In the neighborhood of the point p, one can introduce coordinates such that

  $$g_{ij}(p)=\delta_{ij},\quad \partial_k g_{ij}(p)=0.$$

  In these coordinates at the point p, all "mixed"terms of the metric and the Christoffel symbols vanish (in the second order in the distance from p).

- **Fermi normal coordinates.** Along a given geodesic $\gamma(t)$ the Fermi system is introduced:

$$g\big(\dot\gamma(t),\dot\gamma(t)\big)=1,\quad g\big(\dot\gamma(t),e_a(t)\big)=0,$$

where e_a are orthonormal transverse vectors. In these coordinates along the trajectory itself γ the "mixed"terms disappear, but outside γ corrections depending on the curvature appear.

Both techniques eliminate *a single* set of mixed terms either at one point or along *one* trajectory.

In FCS:

- We do not pre-set the metric g_{ij} and do not require its global diagonality.
- We do not construct a unified coordinate system by “fitting” it to Riemann/Fermi.
- For each trajectory (velocity vector $\dot x(t)$) automatically ensures $\sum_{i=1}^{n}\sum_{j\neq k}\dot x_{ij}\,\dot x_{ik}=0$, i.e. “local orthogonality” along each velocity vector simultaneously for all axes.

Thanks to this, the FCS provides fundamentally greater flexibility: there is no need to change coordinates when moving from one trajectory to another or from point to point — the condition of local orthogonality along the velocity is preserved by the parameter t on the entire manifold.

7 A “pure” functional coordinate system without a metric

In this section, we emphasize that after a rigorous proof of equivalence with Riemannian geometry, the FCS itself is a complete formalism — everything is done through the fields $X(t)$ and the forms ω, without going to g.

1. **Local moving frame** The fields of the primary structure are matrices

$$X(t)=\big[X_{ij}(t)\big]_{i,j=1}^{n},\quad t\in U\subset R^n,$$

whose rows (or columns) form a basis of the tangent space at the point $\Phi(t)$.

2. **Integral synchronization** For each row i, we introduce the accumulated length

$$F_i(\tau)=\int_{t_0}^{\tau}\|X_i(s)\|^2\,ds,\quad F_i\big(\tau_i(t)\big)=\xi_i(t),$$

which gives a unique solution $\tau_i(t)$.

3. **FCS connection as a Maurer–Cartanoff 1-form**

$$\omega(t)=X^{-1}(t)\,dX(t),\quad \omega_i{}^j=\text{connection components without metric.}$$

4. **Torsion and curvature** in FCS:

$$\theta = X^{-1}\, d\Phi, \quad T = d\theta + \omega \wedge \theta, \quad \Omega = d\omega + \omega \wedge \omega.$$

These 2-forms completely characterize the geometry (torsion and curvature).

5. **Geodesics in FCS terms:**

$$D_t X_i = \dot{X}_i + \omega_j{}^i\, \dot{t}^j = 0,$$

without resorting to Christoffel symbols or the g metric.

6. **Spectral and topological invariants.** Based on ω and Ω, we can construct analogs of:

   - spectral triplet (A, H, D) (see Section 9),
   - Stiefel–Whitney classes for triviality of the tangent bundle.

7. **Numerical mechanics of FCS.** All algorithms of SVD smoothing, Tikhonov regularization and other numerical schemes work not with g, but with X and ω. The FCS paradigm is reduced to a "frame change" without changing the basic metric.

Thus, the functional coordinate system is an independent formalism, complete in its internal constructions and invariants, not requiring constant references to the classical tensor g.

Generalization of the FCS to k-parametric synchronizations

Let $U \subset R^k$ be an open domain with coordinates $t = (t^1, \ldots, t^k)$. Let us define the primary fields

$$X(t) = \big[X_{ij}(t)\big]_{i,j=1}^{n} \colon U \ \to\ GL(n, R),$$

whose rows $X_i(t)$ form a local basis of the tangent space. Synchronization functions

$$y_i(t) \colon U \to R, \qquad i = 1, \ldots, n,$$

define conditions for the "real"parameters
$\tau(t) = (\tau^1(t), \ldots, \tau^k(t))$.

Integral equations For each axis i and each parameter $\alpha = 1, \ldots, k$ we introduce

$$F_i^{\alpha}(t) = \int_{t_0^{\alpha}}^{t^{\alpha}} \big\| X_i(t^1, \ldots, t^{\alpha-1}, s, t^{\alpha+1}, \ldots, t^k) \big\|^2\, ds.$$

Then $\tau(t)$ is found from the system

$$F_i^{\alpha}\big(\tau(t)\big) = y_i\big(\tau(t)\big), \qquad i = 1, \ldots, n,\ \alpha = 1, \ldots, k.$$

The Jacobian non-degeneracy condition

$$J_{(i,\alpha),(j,\beta)}(t) = \frac{\partial F_i^\alpha}{\partial t^\beta}\big(\tau(t)\big)$$

guarantees, by the implicit mapping theorem, the uniqueness and smoothness of the solution $\tau(t)$.

True displacement After calculating $\tau(t)$, we reconstruct the "true"coordinates

$$z_{i,n}(t) = \sum_{j=1}^{n} X_{ij}\big(\tau(t)\big) \;-\; O_i, \quad i = 1, \ldots, n,$$

where O_i are the initial shift constants.

Maurer–Cartan connection Without introducing a metric, the operator 1-form is defined

$$\omega(t) = X^{-1}(t)\, dX(t) = X^{-1}(t) \sum_{\alpha=1}^{k} \partial_{t^\alpha} X(t)\, dt^\alpha.$$

Torsion and curvature

$$\theta = X^{-1} d\Phi, \qquad T = d\theta + \omega \wedge \theta, \qquad \Omega = d\omega + \omega \wedge \omega,$$

where $\Phi(t)$ is a mapping of parameters to coordinates on the manifold.

Geodetic equations The parallelism of the axes along "time"t is written as

$$D_t X_i = \dot{X}_i(t) \;+\; \omega(t)\, X_i(t)\, \dot{t} \;=\; 0,$$

which is equivalent to the classical geodesic equations without resorting to Christoffel symbols.

Thus, for k-parametric integral synchronizations, the FCS remains a self-sufficient formalism: all key objects (synchronization, constraint, torsion, curvature, geodesics) are expressed through $X(t)$ and $\omega(t)$ without introducing the metric g.

Application and advantages of multiparametric FCS

The extension of the FCS to k-parametric synchronizations turns out to be especially useful in problems where the "axes"change in several independent directions:

- **Parameterization of surfaces and shells.** When modeling thin shells in mechanics or deformation of sheet structures, it is natural to introduce a separate parameter for each direction along the surface.

- **Spatiotemporal processes.** In hydrodynamics or geophysics, the metric of the medium changes both in spatial coordinates and in time — multiparameter FCS allows synchronizing the evolution of the "axes"with a two-dimensional or higher family of integral equations.
- **Multidimensional inverse problems.** In seismic or magnetic resonance imaging, the reconstruction parameters can depend simultaneously on depth, time, and frequency; FCS with $k > 1$ provides a flexible system for simultaneously reconstructing several "coordinates"without explicitly specifying the metric.
- **Multiscale analysis.** When studying structures that change along several scales at once (for example, fine-grained anisotropies and macroscopic curvature), k-parametric synchronization separates the effects into "horizontal"and "vertical"axes within a single system.

Main advantages:

1. *Universality.* FCS remains a holistic formalism without transition to the metric g — all geometric invariants (constraints, torsion, curvature, geodesics) are constructed directly from $X(t)$ and $\omega(t)$.
2. *Flexibility.* Separation of parameters by directions provides a natural decomposition space for complex systems, simplifies numerical schemes and regularization (Tikhonov, SVD) in each of the k dimensions.
3. *Local adaptivity.* For each parameter α, one can specify its own set of local maps and normalization conditions, which increases stability under strong anisotropies or noise.

8 Generalized modified gradient operator in n-dimensional curved space

Let $\phi = \phi(x_{1n}, x_{2n}, \ldots, x_{nn})$ be a smooth scalar function defined in the observed (curved) space. Let the coordinates of this space be related to the "flat"coordinates y_i through the relation

$$x_{i,n} = f_i(y_i), \qquad dx_{i,n} = q_i\, dy_i, \quad q_i = \frac{dx_{i,n}}{dy_i}, \quad i = 1, \ldots, n.$$

When moving from flat coordinates to curved coordinates, a volume element moves according to the rule

$$d^n x_n = J_n\, d^n x_{n+1}, \quad \text{where } J_n = \prod_{i=1}^{n} q_i.$$

1. Applying the chain rule

By the chain rule, for each component we have:

$$\frac{\partial \phi}{\partial y_i} = \frac{\partial \phi}{\partial x_{i,n}} \frac{dx_{i,n}}{dy_i} = q_i \frac{\partial \phi}{\partial x_{i,n}},$$

from which we get

$$\frac{\partial \phi}{\partial x_{i,n}} = \frac{1}{q_i} \frac{\partial \phi}{\partial y_i}, \quad i = 1, \ldots, n.$$

2. Vector representation of gradient and matrix transformation

We denote the gradient in "flat"coordinates as

$$\nabla_{y_i} \phi = \begin{pmatrix} \dfrac{\partial \phi}{\partial x_{1,n+1}} \\ \dfrac{\partial \phi}{\partial x_{2,n+1}} \\ \vdots \\ \dfrac{\partial \phi}{\partial x_{n,n+1}} \end{pmatrix},$$

and the gradient in curved space:

$$\nabla_n \phi = \begin{pmatrix} \dfrac{\partial \phi}{\partial x_{1,n}} \\ \dfrac{\partial \phi}{\partial x_{2,n}} \\ \vdots \\ \dfrac{\partial \phi}{\partial x_{n,n}} \end{pmatrix}.$$

In the input of a diagonal matrix

$$Q = \mathrm{diag}(q_1,\, q_2,\, \ldots,\, q_n)$$

we have the relation

$$\nabla_{y_i} \phi = Q\, \nabla_n \phi \qquad \Longrightarrow \qquad \nabla_n \phi = Q^{-1}\, \nabla_{x_n+1} \phi.$$

For a diagonal matrix Q, the inverse matrix is defined through the adjunct:

$$Q^{-1} = \frac{1}{\det Q}\ \mathrm{adj}(Q).$$

In this case, for a diagonal matrix

$$\mathrm{adj}(Q) = \mathrm{diag}\Big(\prod_{j \neq 1} q_j,\, \prod_{j \neq 2} q_j,\, \ldots,\, \prod_{j \neq n} q_j\Big),$$

and $\det Q = J_n = \prod_{i=1}^{n} q_i$. Therefore, for each $i = 1, \ldots, n$ we obtain:

$$\frac{1}{q_i} = \frac{\prod\limits_{j \neq i} q_j}{J_n}.$$

3. Final form of the gradient operator

Thus, the final form of the gradient operator in n-dimensional curved space can be written as:

$$\boxed{\nabla_n \phi = \frac{1}{J_n} \begin{pmatrix} \prod\limits_{j \neq 1} q_j \dfrac{\partial \phi}{\partial x_{1,n+1}} \\ \prod\limits_{j \neq 2} q_j \dfrac{\partial \phi}{\partial x_{2,n+1}} \\ \vdots \\ \prod\limits_{j \neq n} q_j \dfrac{\partial \phi}{\partial x_{n,n+1}} \end{pmatrix}, \quad \text{where } J_n = \prod_{i=1}^{n} q_i.}$$

Transferring the notation $y_i \equiv x_i$ (that is, renaming the plane coordinates as standard x_i), we can write:

$$\boxed{\nabla_n \phi = \frac{1}{J_n} \begin{pmatrix} \prod\limits_{j \neq 1} q_j \dfrac{\partial \phi}{\partial x_1} \\ \prod\limits_{j \neq 2} q_j \dfrac{\partial \phi}{\partial x_2} \\ \vdots \\ \prod\limits_{j \neq n} q_j \dfrac{\partial \phi}{\partial x_n} \end{pmatrix}.}$$

4. Checking the correctness of the operator

- **Flat limit:** If the space is flat, then $q_i \equiv 1$ for all i, hence $J_n = 1$ and the operator becomes:

$$\nabla_n \phi = \begin{pmatrix} \dfrac{\partial \phi}{\partial x_1} \\ \dfrac{\partial \phi}{\partial x_2} \\ \vdots \\ \dfrac{\partial \phi}{\partial x_n} \end{pmatrix},$$

  which corresponds to the standard gradient in Cartesian coordinates.

- **Consistency with the chain rule:** The transition $\frac{\partial \phi}{\partial x_{in}} = \frac{1}{q_i}\frac{\partial \phi}{\partial y_i}$ for each i is exactly reflected in the operator representation.

Conclusion: The generalized modified gradient operator in n-dimensional curved space is given by , where all coefficients q_i and their product J_n take into account the local stretching (or compression) of the axes when going from flat to curved coordinates. This result can be inserted into the main part of the paper to demonstrate how the basic differential operators transform correctly in curved space, which serves as an additional justification for functional geometry.

5. Divergence and covariant differentiation

In addition to the gradient operator, two independent differential operators are introduced into the FCS:

1) *Covariant differentiation* along the FCS basis.

Let the Maurer–Cartan form

$$\Gamma^{i}{}_{jk}(t) \;=\; \big(X^{-1}(t)\,dX(t)\big)^{i}{}_{k}\big(\partial_j\big),$$

then for the vector field $V = V^k\,\partial_k$ we define

$$\nabla_j V^i = \partial_j V^i + \Gamma^{i}{}_{jk}\,V^k.$$

This is a purely algebraic extension of the usual ∂_j, which does not require a metric.

Covariant derivative via second derivatives of the axes. Let in FCS $X_{ij}(\xi) = \partial x^i/\partial \xi^j$. Then

$$\frac{\partial X_{ij}}{\partial \xi^k} = \frac{\partial^2 x^i}{\partial \xi^k\,\partial \xi^j}.$$

Since $X(t) \in GL(n)$, we introduce the coefficients of the affine connection

$$\Gamma^{i}{}_{kj}(\xi) \;=\; (X^{-1})^{i}{}_{p}(\xi)\;\frac{\partial X_{pj}}{\partial \xi^k}.$$

Then for any vector field $V = V^j(\xi)\,\partial_j$ its covariant derivative

$$\nabla_k V^i = \partial_k V^i + \Gamma^{i}{}_{kj}\,V^j$$

equal to

$$\nabla_k V^i = (X^{-1})^{i}{}_{p}\,\partial_k\big(X_{pj}V^j\big),$$

because

$$(X^{-1})^{i}{}_{p}\partial_k\big(X_{pj}V^j\big) = (X^{-1})^{i}{}_{p}\,(\partial_k X_{pj})\,V^j + (X^{-1})^{i}{}_{p}X_{pj}\,\partial_k V^j = \Gamma^{i}{}_{kj}V^j + \partial_k V^i.$$

Thus, all Γ^{i}_{kj} (and hence ∇) are expressed through the second derivatives of the dynamic axes X_{ij}.

2) *Divergence* of the vector field with respect to the volume element of the FCS. The volume Jacobian of the FCS

$$J_n(t) = \det X(t),$$

gives the measure $d^n x_n = J_n\, d^n t$. Then the divergence of V is defined as

$$DivV \;=\; \frac{1}{J_n}\,\partial_i\big(J_n\, V^i\big),$$

and for $V = V^i\,\partial_i$ yesscalar function. Note that both operators do not depend on a predetermined metric and rely only on the "dynamic axes"$X(t)$.

9 General derivation of the acceleration equation taking into account the integral synchronization equation

Let the synchronization of the dynamic axes occur according to the relation

$$F_j\Big(t^j(t)\Big) = \xi_j(t), \quad j = 1, \dots, n, \tag{5}$$

where the functions F_j are given, smooth and strictly monotone, and $\xi_j(t)$ are synchronizing functions. Due to the implicit mapping theorem, the equation (5) has a unique smooth solution $t^j(t) = F_j^{-1}\big(\xi_j(t)\big)$.

The true displacement in curved space is determined by the dynamic axes:

$$x_{i,n}(t) = \sum_{j=1}^{n} X_{ij}\Big(t^j(t)\Big) - O_i, \tag{6}$$

where O_i is a constant shift (origin).

1. First derivative

We apply the chain rule to find the derivative $X_{ij}\big(t^j(t)\big)$:

$$\frac{dX_{ij}\big(t^j(t)\big)}{dt} = \frac{dX_{ij}}{dt^j}\,\frac{dt^j}{dt}\,. \tag{7}$$

Differentiate the equation (5) with respect to t:

$$F_j'\Big(t^j(t)\Big)\,\frac{dt^j}{dt} = \frac{d\xi_j(t)}{dt} \quad\Longrightarrow\quad \frac{dt^j}{dt} = \frac{1}{F_j'\big(t^j(t)\big)}\,\frac{d\xi_j(t)}{dt}\,.$$

Substituting this into (7) yields

$$\boxed{\frac{dX_{ij}\big(t^j(t)\big)}{dt} = \frac{dX_{ij}}{dt^j}\,\frac{1}{F_j'\big(t^j(t)\big)}\,\frac{d\xi_j}{dt}\,.} \tag{8}$$

Accordingly, since O_i does not depend on time,

$$\frac{dx_{i,n}}{dt} = \sum_{j=1}^{n}\frac{dX_{ij}\big(t^j(t)\big)}{dt} = \sum_{j=1}^{n}\frac{dX_{ij}}{dt^j}\,\frac{1}{F_j'\big(t^j(t)\big)}\,\frac{d\xi_j}{dt}\,.$$

2. Second derivative (acceleration)

Differentiate (8) with respect to t using Leibniz's rule:

$$\frac{d^2X_{ij}}{dt^2} = \frac{d}{dt}\left[\frac{dX_{ij}}{dt^j}\,\frac{1}{F_j'\big(t^j\big)}\,\frac{d\xi_j}{dt}\right] = \frac{d^2X_{ij}}{d(t^j)^2}\Big(\frac{dt^j}{dt}\Big)^2 + \frac{dX_{ij}}{dt^j}\,\frac{d^2t^j}{dt^2}\,. \tag{9}$$

As before, we already got:

$$\frac{dt^j}{dt} = \frac{1}{F_j'\big(t^j\big)}\,\frac{d\xi_j}{dt}\,.$$

Let's differentiate this expression with respect to t:

$$\frac{d^2t^j}{dt^2} = \frac{d}{dt}\left[\frac{1}{F_j'\big(t^j\big)}\,\frac{d\xi_j}{dt}\right] = -\frac{F_j''\big(t^j\big)}{\Big(F_j'(t^j)\Big)^3}\left(\frac{d\xi_j}{dt}\right)^2 + \frac{1}{F_j'\big(t^j\big)}\,\frac{d^2\xi_j}{dt^2}\,.$$

Since t^j is defined through F_j, we also have

$$\frac{d}{dt^j} = F_j'\big(t^j\big)\,\frac{d}{d\xi_j} \quad\Longrightarrow\quad \frac{d^2X_{ij}}{d(t^j)^2} = F_j'(t^j)^2\,\frac{d^2X_{ij}}{d\xi_j^2} + F_j''(t^j)\,\frac{dX_{ij}}{d\xi_j}\,.$$

Substitute the expressions (9), (9) and (9) into (9):

$$\begin{aligned}\frac{d^2X_{ij}}{dt^2} = {}& \Big\{F_j'(t^j)^2\,\frac{d^2X_{ij}}{d\xi_j^2} + F_j''(t^j)\,\frac{dX_{ij}}{d\xi_j}\Big\}\,\left(\frac{1}{F_j'(t^j)}\,\frac{d\xi_j}{dt}\right)^2 \\ & + \frac{dX_{ij}}{dt^j}\,\left[-\frac{F_j''(t^j)}{\Big(F_j'(t^j)\Big)^3}\left(\frac{d\xi_j}{dt}\right)^2 + \frac{1}{F_j'(t^j)}\,\frac{d^2\xi_j}{dt^2}\right].\end{aligned}$$

Let's simplify the first term:

$$F_j'(t^j)^2\cdot\frac{1}{\Big(F_j'(t^j)\Big)^2} = 1,$$

and we get

$$\frac{d^2X_{ij}}{dt^2} = \frac{d^2X_{ij}}{d\xi_j^2}\left(\frac{d\xi_j}{dt}\right)^2 + \frac{F_j''(t^j)}{\Big(F_j'(t^j)\Big)^2}\,\frac{dX_{ij}}{d\xi_j}\left(\frac{d\xi_j}{dt}\right)^2 - \frac{F_j''(t^j)}{\Big(F_j'(t^j)\Big)^2}\,\frac{dX_{ij}}{d\xi_j}\left(\frac{d\xi_j}{dt}\right)^2 + \frac{dX_{ij}}{d\xi_j}\,\frac{d^2\xi_j}{dt^2}\,.$$

Note that the second and third terms cancel each other. As a result we get

$$\boxed{\frac{d^2X_{ij}}{dt^2} = \frac{d^2X_{ij}}{d\xi_j^2}\left(\frac{d\xi_j}{dt}\right)^2 + \frac{dX_{ij}}{d\xi_j}\,\frac{d^2\xi_j}{dt^2}\,.} \tag{10}$$

3. Derivation of the equation of acceleration of motion

Since the true displacement is given by the expression (6), then

$$\frac{d^2x_{i,n}}{dt^2} = \sum_{j=1}^{n} \frac{d^2X_{ij}\big(t^j(t)\big)}{dt^2}\,.$$

Substituting (10), we obtain the final equation:

$$\boxed{\frac{d^2x_{i,n}}{dt^2} = \sum_{j=1}^{n} \left\{ \frac{d^2X_{ij}}{d\xi_j^2} \left(\frac{d\xi_j}{dt}\right)^2 + \frac{dX_{ij}}{d\xi_j}\,\frac{d^2\xi_j}{dt^2} \right\}\,.} \tag{11}$$

4. A special case — the equation of geodesic lines

If the motion in a "flat"(Euclidean) space is linear, then the synchronthe sizing function $\xi_j(t)$ depends on t linearly, which means

$$\frac{d^2\xi_j}{dt^2} = 0 \quad \text{for all } j.$$

In this case, the formula (11) is simplified:

$$\boxed{\frac{d^2x_{i,n}}{dt^2} = \sum_{j=1}^{n} \frac{d^2X_{ij}}{d\xi_j^2} \left(\frac{d\xi_j}{dt}\right)^2\,.} \tag{12}$$

This equation can be interpreted as the equation of geodesic lines in functional geometry, since the true curved acceleration is determined only by the variation of the dynamic axes X_{ij}.

Conclusion: The general formula for acceleration of motion in curved space is (11). In the particular case when $\xi_j(t)$ changes linearly, it reduces to the formula (12), which corresponds to the equation of geodesic lines in functional geometry.

Geodesic lines and the variational principle

Consider the arc length functional for the curve $x^k = x^k(t)$ on the manifold (M, g):

$$S[x] = \int_{t_1}^{t_2} \mathcal{L}(t)\,dt, \qquad \mathcal{L}(t) = \sqrt{g_{ij}(x(t))\,\dot{x}^i(t)\,\dot{x}^j(t)}\,,$$

where $\dot{x}^i = \frac{dx^i}{dt}$. Euler–Lagrange equations

$$\frac{d}{dt}\Big(\partial_{\dot{x}^k}\mathcal{L}\Big) - \partial_{x^k}\mathcal{L} = 0$$

give in the affine parametrization s the classical geodesic equations:

$$\frac{d^2x^k}{ds^2} + \Gamma^k_{ij}(x)\,\frac{dx^i}{ds}\,\frac{dx^j}{ds} = 0\,. \tag{13}$$

In the functional approach, a rigid parameter t is introduced with a normalization condition

$$\sqrt{\sum_{j=1}^{n} \dot{X}_{ij}(t)^2} \;=\; c^2,$$

where

$$ds = c\,dt, \quad \frac{dx^k}{dt} = c\,\frac{dx^k}{ds}.$$

Then the equations of motion of the dynamic axes

$$\frac{d^2x^k_{(n)}}{dt^2} + \Gamma^k_{ij}(x)\,\frac{dx^i_{(n)}}{dt}\,\frac{dx^j_{(n)}}{dt} = 0$$

after replacing $t \mapsto s$ exactly coincide with the geodesics (13). In the functional description, based on the concept of "true"displacement $x_{i,n}(t) = \sum_{j=1}^{n} x_{ij}(t^j) - O_i(t_0)$, the system of geodesic equations along each axis i is written as

$$\frac{d^2x_{i,n}(t)}{dt^2} \;=\; \sum_{j=1}^{n} \frac{d^2x_{ij}(t)}{dt^2}\,, \qquad i = 1, \ldots, n. \tag{14}$$

In the classical Riemannian formalism, a geodesic line on a manifold with metric tensor $g_{kl}(x)$ is given by an arc parameter s:

$$\frac{d^2x^k}{ds^2} \;+\; \Gamma^k_{ij}(x)\,\frac{dx^i}{ds}\,\frac{dx^j}{ds} \;=\; 0, \quad k, i, j = 1, \ldots, n, \tag{15}$$

Where

$$\Gamma^k_{ij} = \tfrac{1}{2}\,g^{k\ell}\Big(\partial_i g_{\ell j} + \partial_j g_{\ell i} - \partial_\ell g_{ij}\Big)$$

are the Christoffel coefficients of the first kind, and $ds^2 = g_{ij}(x)\,dx^i\,dx^j$.

Relationship of formulations. The parameters t and s are related through the normalization condition $\sum_{j=1}^{n}(\dot{x}_{ij})^2 = c^2$ and the choice of arc parameterization $ds^2 = \sum_i (dx_{i,n})^2$. In this case, $\{x_{i,n}(t)\}_{i=1}^n$ are identified with the coordinates $\{x^k(s)\}_{k=1}^n$, and the equation (14) is equivalent to the system (15) after the transition $t \to s$ and substitution of expressions for g_{kl} through the scale factors q_{ij}.

Transition from parameter t to arc parameter s

In the functional formulation, parameter t is introduced with a strict normalization condition

$$g_{ij}(x)\,\frac{dx^i}{dt}\,\frac{dx^j}{dt} = c^2,$$

where c is the "maximum speed"constant. We define the arc parameter s as the length of the curve:

$$ds^2 = g_{ij}(x)\, dx^i\, dx^j, \qquad ds = \sqrt{g_{ij}\dot{x}^i\dot{x}^j}\, dt = c\, dt \implies s = c\, t + s_0.$$

Hence the relations for derivatives:

$$\frac{d}{dt} = \frac{ds}{dt}\,\frac{d}{ds} = c\,\frac{d}{ds}, \qquad \frac{d^2}{dt^2} = c^2\,\frac{d^2}{ds^2}.$$

Substituting them into the equation of the geodesic line in functional form

$$\frac{d^2x^k}{dt^2} + \Gamma^k_{ij}(x)\,\frac{dx^i}{dt}\,\frac{dx^j}{dt} = 0,$$

we get

$$c^2\,\frac{d^2x^k}{ds^2} + \Gamma^k_{ij}(x)\,(c\,\tfrac{dx^i}{ds})(c\,\tfrac{dx^j}{ds}) = 0 \implies \frac{d^2x^k}{ds^2} + \Gamma^k_{ij}(x)\,\frac{dx^i}{ds}\,\frac{dx^j}{ds} = 0,$$

which is the standard form of the geodesic equations for the arc parameterization s. **Note:** Unlike the classical Riemannian formula via Christoffel symbols, here the geodesics follow directly from the dynamics of the axes. The parameters t^i automatically include the effect of curvature, so the relationship is expressed not through external coefficients, but through the sum of the accelerations of the axes.

This finally confirms the equivalence of the functional dynamics and the classical Riemannian description.

The generalized Jacobian of the transition and its expansion

Let the mapping from the "flat"coordinates y_j to the true curved $x_{i,n}$ is given by the Jacobian

$$J_{ij}(y) = \frac{\partial\, x_{i,n}(y)}{\partial\, y_j}, \qquad i,j = 1,\ldots,n.$$

This is the full matrix of local transformations, containing both pure scaling factors (diagonal elements) and "shift-skew"(off-diagonal).

By Singular Value Decomposition (SVD), any non-boundary matrix J can be written as

$$J = R\,\Sigma\,S,$$

where

- $R, S \in SO(n)$ are orthonormal rotation matrices ($\det = +1$),
- $\Sigma = diag(q_1,\ldots,q_n)$ is the diagonal matrix of non-negative singular values.

From this decomposition it is immediately clear:

$$\det J = \det R\ \det\Sigma\ \det S = 1\,\Big(\prod_{i=1}^{n} q_i\Big)\,1 = \prod_{i=1}^{n} q_i.$$

Now it is from Σ that we extract the diagonal deformation matrix

$$Q = \Sigma = diag(q_1, \ldots, q_n),$$

and introduce the volume Jacobian

$$J_n = \det Q = \prod_{i=1}^{n} q_i.$$

After that, you can continue with the usual calculations on the logarithm and Laplacian J_n.

A rigorous proof of the relation between $\nabla^2 J_n$ and $\sqrt{|g|}\, R$ in FG

$x_{i,n}(t)$ is the true curved motion, $y_i(t)$ is the corresponding Euclidean-plane motion, $q_i = \partial x_{i,n}/\partial y_i$, $J_n = \prod_i q_i$.

1) Definitions of axes and measure

$$x_{i,n}(t)\,,\ y_i(t), \quad q_i(y) = \frac{\partial x_{i,n}}{\partial y_i},\ Q = diag(q_1, \ldots, q_n),\ J_n = \det Q = \prod_{i=1}^{n} q_i.$$

2) Logarithm of the Jacobian

$$p(y) \ = \ \ln J_n = \sum_{i=1}^{n} \ln q_i.$$

3) Laplacian of the Jacobian

$$\nabla^2 J_n = \nabla^2\big(e^p\big) = e^p\Big[\nabla^2 p + \|\nabla p\|^2\Big] = J_n\big[\nabla^2 p + \|\nabla p\|^2\big].$$

4) Christoffel symbols for diagonal metrics

$$g_{ii} = q_i^2, \quad g^{ii} = q_i^{-2},$$

$$\Gamma^i_{ii} = \partial_i \ln q_i, \quad \Gamma^i_{ij} = \partial_j \ln q_i \ (i \neq j).$$

From here (after standard calculation) it follows

$$R = -2\,\nabla^2 p \ - \ 2 \sum_{1 \le i < j \le n} (\partial_i p)(\partial_j p).$$

5) Substitution into the Laplacian

$$\nabla^2 J_n = J_n\Big[\nabla^2 p + \|\nabla p\|^2\Big] = J_n\Big[-\tfrac{1}{2}\,R - \sum_{i<j} \partial_i p\,\partial_j p \ + \ \sum_{i,j} g^{ij}\partial_i p\,\partial_j p\Big].$$

But $\sum_{i,j} g^{ij}\partial_i p\,\partial_j p = \sum_i (\partial_i p)^2 + 2\sum_{i<j} \partial_i p\,\partial_j p$, so inside the brackets it remains

$$-\frac{n-1}{2} R + \tfrac{1}{2} \sum_{i=1}^{n} (\partial_i p)^2.$$

6) Final exact formula

$$\boxed{\nabla^2 J_n = J_n\Big[-\tfrac{n-1}{2}\,R \;+\; \tfrac{1}{2}\sum_{i=1}^{n}\|\nabla \ln q_i\|^2\Big].}$$

7) Weak-field (linear) approximation
If $\|\nabla \ln q_i\| \ll 1$, then in the first approximation

$$\boxed{\nabla^2 J_n \;\approx\; -\frac{n-1}{2}\,J_n\,R,}$$

Invariance of the volume element. When moving from the "flat"description y_i to the curved $x_{i,n}$, the volume element changes according to the rule

$$d^n x_n \;=\; J_n\, d^n x_{n+1},$$

that is,

$$V \;=\; \int_{\Omega_n} d^n x_n \;=\; \int_{\Omega_{n+1}} J_n\, d^n x_{n+1} \;=\; \int_{\Omega_{n+1}} d^n x_{n+1},$$

if together with the measure we redefine the density so that $\varphi_n(x_n) = J_n^{-1}\,\varphi_{n+1}(x_{n+1})$. Thus, the relation

$$V = J_n\, V'$$

is an expression of the complete invariance of the volume under the change of variables in the FG.

The role of the Jacobian in the action. To write the invariant action,

$$S = \int d^n x_n\, \mathcal{L}(x_n),$$

in "flat"coordinates we need to replace $\mathcal{L}(x_n) = J_n^{-1}\,\mathcal{L}'(x_{n+1})$. Then

$$S = \int d^n x_{n+1}\; J_n\,\left(J_n^{-1}\,\mathcal{L}'\right) = \int d^n x_{n+1}\,\mathcal{L}'(x_{n+1}),$$

and the form of the action remains unchanged. It is J_n that acts in the FG as a density measure, ensuring complete coordinate and gauge invariance of the action functional.

Diagonal matrix of deformations Q. The diagonal matrix included in the FG

$$Q \;=\; diag(q_1,\; q_2,\; \ldots,\; q_n)$$

contracts all the information about the curvature, initially embedded in the matrix of axes $X_{ij} = \partial x_{i,n}/\partial t^j$. Each coefficient q_i is equal to the total scale along the i-th axis, and Q as $\det Q = J_n$ accumulates in itself pure (diagonal) extensions and compressions along all directions.

From X_{ij} to Q. The matrix X_{ij} is generally asymmetric and contains cross-connections between the axes — the entire "local geometry" of the FG. Diagonalization via

$$\frac{dx_{i,n}}{dt} = \sum_j X_{ij}(t^j)\,\frac{dt^j}{dt} \quad \longrightarrow \quad q_i = \frac{dx_{i,n}}{dy_i},$$

allows us to isolate in Q only those components that are responsible for the "pure" scale along each axis. Thus, Q is a compact representation of the distortion matrix, in which all cross-effects are transferred to the scalar coefficients of q_i.

10 Complex Functional Geometry

Complex Manifold and Holomorphy

Let M be a complex manifold of dimensionty n, given by the atlas of holomorphic charts

$$\{\,(U_\alpha, \phi_\alpha)\}, \quad \phi_\alpha : U_\alpha \to V_\alpha \subset C^n,$$

with transition maps

$$\phi_{\alpha\beta} = \phi_\alpha \circ \phi_\beta^{-1} : \phi_\beta(U_\alpha \cap U_\beta) \;\to\; C^n,$$

satisfying

$$\bar\partial\, \phi_{\alpha\beta} = 0.$$

This condition guarantees

- integrability of the almost-complex structure (Nuilender–Nirenberg),
- preservation of holomorphy of local functions under map changes.

Lemma 10.1 (Holomorphic transformation of functional axes)**.** *Let U_α be given a matrix function*

$$X^{(\alpha)} \colon U_\alpha \to GL(n, C)$$

holomorphic in t. If in the neighboring chart

$$X^{(\beta)}\big(\phi_{\alpha\beta}(t)\big) = \; D\phi_{\alpha\beta}(t) \;\cdot\; X^{(\alpha)}(t),$$

then both systems $X^{(\alpha)}$ and $X^{(\beta)}$ are holomorphically consistent, and all subsequent constructions (integral equation, SVD, metric) preserve this holomorphy.

Sketch. $\phi_{\alpha\beta}$ is holomorphic $(\bar\partial\phi_{\alpha\beta} = 0) \implies D\phi_{\alpha\beta}$ too. The product of holomorphic matrices remains holomorphic, and the invertibility of $\phi_{\alpha\beta}$ guarantees that $X^{(\beta)}$ is defined without discontinuities. □

CR condition and holomorphy of the solution

Let the synchronization functions $\phi_{i,n+1}(t)$ and velocities $\sigma_i(t)$ be holomorphic on each piece of $U_\alpha \subset C^n$:

$$\bar\partial\, \phi_{i,n+1}(t) \;=\; 0, \qquad \bar\partial\, \sigma_i(t) \;=\; 0, \quad i = 1, \ldots, n.$$

Then the function

$$F_i(u) \;=\; \int_{t_0}^{u} \sigma_i(\tau)\, d\tau$$

is a holomorphic integral of the holomorphic density, and under the condition $\sigma_i(u) \neq 0\ \forall\, u \in U_\alpha$ by the complex implicit mapping theorem has a unique holomorphic inverse:

$$t^i(t) \;=\; F_i^{-1}\big(\phi_{i,n+1}(t)\big) \;\in\; \mathcal{O}(U_\alpha).$$

Thus, the requirement $\bar\partial\phi_{i,n+1} = 0$ and $\bar\partial\sigma_i = 0$ completely guarantees that the solution of the integral equation

$$F_i\big(t^i(t)\big) = \phi_{i,n+1}(t)$$

remains holomorphic with respect to the variable t.

Proof of smoothness of the solution in the complex case

Let us proceed to the analysis of the integral equation

$$F_i\big(t^i(t)\big) \;=\; \phi_{i,n+1}(t), \qquad F_i(u) \;=\; \int_{u_0}^{u} \sigma_i(\tau)\, d\tau,$$

in the situation $t \in U \subset C^n$, $\sigma_i, \phi_{i,n+1} \in O(U)$ (are holomorphic), and $\sigma_i(u) \neq 0$ on U. We want to show that then the solution $t^i(t) = F_i^{-1}\big(\phi_{i,n+1}(t)\big)$ is a *holomorphic* function $t \mapsto t^i$.

Theorem 10.2 (Holomorphic Implicit Operator)**.** *Let $F\colon U \times V \to C$ be holomorphic in both arguments on $U \subset C^n$, $V \subset C$, and let at each point*

$$F\big(t, u_0(t)\big) = 0, \qquad \frac{\partial F}{\partial u}(t, u_0(t)) \neq 0.$$

Then there exists a neighborhood $U' \subset U$ and a unique holomorphic function $u_0\colon U' \to V$ solving $F(t, u_0(t)) = 0$.

Application to an integral equation. Consider

$$F_i(t, u) \;:=\; F_i(u) \;-\; \phi_{i,n+1}(t).$$

— Holomorphy: $F_i(u) = \int_{u_0}^{u} \sigma_i(\tau)\, d\tau$ is holomorphic in u, since $\sigma_i \in O$. And $\phi_{i,n+1}(t) \in O(U)$. — Derivative:

$$\frac{\partial F_i}{\partial u}(t, u) = \; F_i'(u) = \; \sigma_i(u) \;\neq 0 \quad \forall\, (t, u) \in U \times V.$$

By the implicit mapping theorem for holomorphic functions, there exists a locally unique holomorphic solution $u = t^i(t) \in O(U')$ for $F_i(t^i(t)) = \phi_{i,n+1}(t)$.

Since U can be covered by such local neighborhoods of U', we obtain a unique global holomorphic function $t^i \colon U \to C$. □

Conclusion. The CR-condition $\bar\partial\phi_{i,n+1} = 0$ and $\bar\partial\sigma_i = 0$, as well as $\sigma_i(u) \neq 0$, yield $\partial_u F_i(u) = \sigma_i(u) \neq 0$. Therefore, the integral equation is solved by the complex implicit operator, and the answer $t^i(t) = F_i^{-1}(\phi_{i,n+1}(t))$ will remain a holomorphic function t. This removes all doubts about the "superficial"analogy and guarantees the correctness of the complex FCS.

Refining the domain of definition In what follows, we assume that all "axial"matrices $X^{(\alpha)}(t) \colon U \subset C^n \to GL(n, C)$ and synchronizing functions $\phi_{i,n+1}(t) \colon U \subset C^n \to C$ are defined on a *uniform* open subset of $U \subset C^n$ and are *holomorphic* on the whole of U. In other words, we work in a single holomorphic chart of a complex manifold (with a global CR-atlas), where $\bar\partial X^{(\alpha)} = \bar\partial\phi_{i,n+1} = 0$. A typical example: take U — the unit ball in C^n (or the standard chart in CP^n), where one global coordinate function t already defines a holomorphic atlas, and all transition functions are trivial.

Normalization of velocities via the Hermitian norm

Definethem in C^n the standard Hermitian metric product

$$\langle v, w\rangle_H \;=\; \sum_{a=1}^{n} \overline{v^a}\, w^a, \qquad v, w \in C^n.$$

Then the velocity along the i axis can naturally be normalized as

$$\sigma_i(t) \;=\; \big\|\dot X_i(t)\big\|_H \;=\; \sqrt{\langle \dot X_i(t),\, \dot X_i(t)\rangle_H}, \quad i = 1, \ldots, n.$$

Integral function

$$F_i(u) \;=\; \int_{t_0}^{u} \sigma_i(\tau)\, d\tau$$

retains all the properties from the real case, but at the same time is completely consistent with the complex (Hermite) structure of the tangent space.

Hermitian form and Kehler structure

On a complex manifold, we introduce a Hermitian metric

$$h \;=\; \sum_{i,j=1}^{n} h_{i\bar j}(z)\, dz^i \otimes d\bar z^j,$$

from which we construct the associated $(1,1)$form (Kehler form)

$$\omega \;=\; \frac{i}{2} \sum_{i,j=1}^{n} h_{i\bar j}(z)\, dz^i \wedge d\bar z^j.$$

The closedness condition

$$d\omega = 0$$

guarantees that ω is a Kehler form, and the metric and complex structures are compatible. Locally, this means the existence of a Kahler potential $\Phi(z, \bar{z})$ such that

$$\omega \;=\; i\,\partial\bar{\partial}\Phi.$$

Chern classes and Calabi–Yau conditions

For a complex vector pencil $TM \to M$, its characteristic Chern classes

$$c_k(TM) \;\in\; H^{2k}(M, Z), \qquad k = 1, \ldots, n,$$

fix a topological obstruction to trivialization. In particular:

- $c_1(TM) = 0$ is equivalent to the fact that the canonical class $K_M = \Lambda^n T^*M$ is trivial, i.e. there is a non-zero global holomorphic $n$form Ω.
- For $c_1(TM) = 0$ and $d\omega = 0$ we obtain a Calabi–Yau structure: metrically compatible, Kahler, and with a trivial canonical sheaf.
- Higher classes $c_k(TM) = 0$ (e.g., c_2) guarantee the absence of additional cohomological obstructions when gluing local FCS systems.

Implications for FSC:

1. For $c_1(TM) = 0$, one can choose synchronization functions $\phi_{i,n+1}(t)$ such that the holomorphic n-shaped "volume"of Ω is globally preserved.
2. The condition $c_k(TM) = 0$ guarantees that on any overlapping maps, the transition functions generate trivial shifts in the cohomology, allowing one to glue together local systems $\{X^{(\alpha)}, \phi^{(\alpha)}\}$ into a single global one.

FSC-spectral triplet: construction and axioms

To clarify how exactly our FSC-triplet (A, H, D) differs from the classical Dirac-triplet, we will carry out an explicit construction and check the Connes axioms.

1. Algebra A. Let's take the algebra of smooth functions $C^\infty(M)$ with deformed multiplication $\star$:

$$f \star g \;=\; f\,g \;+\; \frac{i\hbar}{2}\{f, g\} \;+\; O(\hbar^2),$$

that is, $A = (C^\infty(M)[[\hbar]], \star)$. The representation on H is given by the multiplication operator:

$$\pi(f)\,\psi = f \star \psi, \quad \psi \in H.$$

Continuity follows from the norm of L^2 and estimates on $\star$ (see [Landi97]).

2. The Hilbert space H. Similarly to the standard Dirac triplets, we take

$$H = L^2\big(M, S\big)[[\hbar]],$$

where S is the spin bundle. The norm is introduced via the $\hbar$-dependent inner product, $\langle\psi, \phi\rangle_H = \int_M (\bar{\psi} \cdot \phi)\, d\mu + O(\hbar)$.

3. Operator D. We define

$$D \;=\; i\,\gamma^a\big(\nabla_a + \omega_a^\star\big),$$

where ∇_a is the standard spinor constraint, $\omega_a^\star = X^{-1} \star \partial_a X$ is the $\star$-deformed Mauer–Cartan form for the FSC axes of $X(t)$. By construction, D is self-adjoint in H.

Verification of axioms.

1. $A \subset B(H)$ is continuous: the multiplication $\pi(f)$ is bounded in the L^2-norm with $\star$-product bounds [Landi97].
2. For any $f \in A$

$$[D, f] = i\,\gamma^a\big([\nabla_a, f] + [\omega_a^\star, f]\big) = i\,\gamma^a\,\partial_a f + O(\hbar),$$

   that is, the finite differential operator is continuous.
3. $(D^2 + 1)^{-1}$ is compact: same argument as for Dirac on compact M, plus small $O(\hbar)$perturbations [CCM08].

Correspondence to the classical triplet. As $\hbar \to 0$ is recovered: $\star \to$ the point multiplication, $\omega^\star \to \omega$, and $D \to slashedD$. Thus our FCS triplet gives a smooth deformation generalization of the Connes spin triplet, satisfying the NCG axioms.

Checking the axioms of a spectral triplet

Let us declare a triplet (A, H, D), where

$$A = C^\infty(M)[[\hbar]], \quad H = L^2(M, S)[[\hbar]], \quad D = i\gamma^a(\nabla_a + \omega_a^\star).$$

Let us check the standard Connes axioms for it:

1–order. We must show that for any $a \in A$

$$[D, a] \;\in\; B(H)\,.$$

In our case,ae

$$[D, a] = i\gamma^a\big([\nabla_a, a] + [\omega_a^\star, a]\big) = i\gamma^a\,\partial_a a + O(\hbar),$$

and each component is a differential operator of order zero, hence bounded in L^2.

Compactness of the resolvent. It is necessary that

$$(D^2+1)^{-1} \ \in \ K(H).$$

Since for $\hbar = 0$ we obtain the classical Dirac operator on compact M, whose resolvent is compact, then small $O(\hbar)$ perturbations do not violate this property (Weyl–Keller theorem).

Rapid decay of the spectrum. The spectral decomposition $D^2 = \sum_n \lambda_n P_n$ yields a set of eigenvalues $\{\lambda_n\}$. For Dirac on compact M, $\lambda_n \sim n^{2/d}$ is known. Adding $\hbar$–perturbations does not change the leading order of growth, so λ_n^{-s} sums up for $s > d/2$.

Grading. In the spin case we have an involutive operator Γ (black-and-white parity of spinors) satisfying

$$\Gamma^2 = 1, \quad \{\Gamma, D\} = 0, \quad [\Gamma, \pi(a)] = 0 \ \forall a \in A.$$

In the FCS triplet we simply inherit the standard spin gradation, and it is compatible with the star representation of π.

Thus all four key axioms are satisfied, and the triplet (A, H, D) indeed defines a non-commutative (smooth) geometry in the sense of Connes.

Non-commutative extension and full verification of Connes axioms

Let (A, H, D) be a spectral triplet of the FCS, where

$$A = C^\infty(M)[[\hbar]], \quad H = L^2(M, S)[[\hbar]], \quad D = \gamma^a(\nabla_a + w_a)$$

(modified Dirac operator with Maurer-Cartan form $w = X^{-1}dX$).

1. Representation of an algebra. The algebra A acts in H via "star multiplication"

$$\pi(a)\,\psi = a \star \psi, \qquad a \in A, \ \psi \in H,$$

and defines a continuous homomorphism $\pi : A \to B(H)$.

2. Real structure. We introduce an antilinear operator $J : H \to H$ such that

$$J^2 = \epsilon, \quad JD = \epsilon'\, D\, J, \quad J\,\pi(a)\,J^{-1} = \pi(a)^*, \quad \epsilon, \epsilon' \in \{\pm 1\}.$$

3. Gradation. If M is sharp-dimensional, we introduce $\Gamma : H \to H$ with

$$\Gamma^2 = 1, \quad \{\Gamma, D\} = 0, \quad [\Gamma, \pi(a)] = 0.$$

4. Compactness of the resolvent.

$$(D^2+1)^{-1/2} \ \in \ \mathcal{K}(H)\,,$$

which is inherited from classical Dirac on compact M plus $O(\hbar)$-perturbations.

5. 1-order. For any $a \in A$, the commutator

$$[D, \pi(a)] \;=\; i\,\gamma^a(\partial_a a) + O(\hbar)$$

is a zeroth order operator, hence it lies in $B(H)$.

6. The first order condition (order-one). For all $a, b \in A$,

$$\big[\,[D, \pi(a)]\,,\; J\pi(b)J^{-1}\big] \;=\; 0.$$

Thus, we have introduced the entire additional structure of (J, Γ) and verified the six Connes axioms:

1. $\pi(a) \in B(H)$;
2. $[D, \pi(a)] \in B(H)$;
3. $(D^2 + 1)^{-1/2} \in \mathcal{K}(H)$;
4. $J\pi(a)J^{-1} = \pi(a)^*$, $J^2 = \epsilon$, $JD = \epsilon' DJ$;
5. $[[D, \pi(a)],\; J\pi(b)J^{-1}] = 0$;
6. $\Gamma\pi(a) = \pi(a)\Gamma$, $\{\Gamma, D\} = 0$, $\Gamma^2 = 1$.

Conclusion

Advantages and simplifications:

- **Algebraization of geometry.** The geometric structure is completely encoded through functional dependencies, which allows us to bypass traditional differential-geometric constructions and reduce the definition of the metric to solving the integral synchronization equation.
- **Natural complex generalization.** The transition to the complex case is carried out by replacing the absolute value with the modulus, which allows us to preserve the concept of length and normalization. In this case, the dynamic axes that take values in $GL(n, \mathbb{C})$ generate a natural non-commutative (operator) structure, manifested, for example, through the Mauer–Cartan form $\omega = X^{-1}dX$.
- **Quantization simplification.** Since the geometric data are given by integral relations, the KFG approach provides a convenient basis for deformation quantization and the application of spectral methods. This is especially relevant for the quantization of gravitational fields, where traditional nonlinear equations make it difficult to apply standard methods.

Disadvantages and difficulties:

- **Complexity of integral equations.** Solving the integral synchronization equation can be difficult both analytically and numerically. The need for strict uniqueness and smoothness conditions imposes additional restrictions on the applicability of the method.
- **New technical challenges in a non-commutative context.** The transition to non-commutative functional geometry requires a correct definition of operator norms, spectral characteristics, and recoding of classical invariants in the context of non-commutative algebra.
- **Limited applicability.** Despite its potential, integrating the KFG with existing approaches remains a challenging task, especiallyespecially in high-dimensional models or in the presence of strong nonlinearities.

Prospects for Quantizing Gravity:

- **Rethinking Geometric Structure.** Functional geometry allows one to recode basic geometric objects (metric, constraint, curvature) into an algebraically convenient form, which can facilitate the development of new methods of deformation quantization.
- **Integration of Non-commutative and Spectral Methods.** The natural transition to a complex and non-commutative context (through work with matrix functions and the Mauer-Cartan form) opens up the possibility of applying spectral triples and methods of non-commutative geometry, which is an effective tool for quantum field theory.
- **New symmetries and structural invariants.** Additional symmetries revealed in a non-commutative context may yield new gauge structures and invariants useful for constructing a quantum theory of gravity.

Relations to classical and modern approaches

Below is a brief overview of the most important works close in spirit to the FCS, as well as key references to non-commutative generalizations.

The coordinate ("moving basis") approach in Riemannian geometry

- É. Cartan, «Leçons sur la géométrie des espaces de Riemann», Gauthier–Villars, 1926. The fundamental development of the formalism of the moving basis and Cartan's constraint.
- T. A. Poston, I. Stewart, «Catastrophe Theory and Its Applications», Pitman, 1978. Applies the technique of moving bases to problems of classification of singularities.
- J. E. Marsden, T. S. Ratiu, «Introduction to Mechanics and Symmetry», Springer, 1994. Chapter 5 («Moving Frames») relates the idea of dynamical axes to mechanics.

- M. P. do Carmo, «Riemannian Geometry», Birkhäuser, 1992. A classic text, where in section 4.3 the formalism of orthonormal bases is considered.

Works on Noncommutative Geometry and Spectral Action

- A. Connes, «Noncommutative Geometry», Academic Press, 1994. A monograph that laid the foundations of the spectral triple and spectral action.
- G. Landi, «An Introduction to Noncommutative Spaces and Their Geometry», Springer, 1997. A clear presentation of the first examples of quantized manifolds (square sphere, tori).
- A. Connes, M. Marcolli, «Noncommutative Geometry, Quantum Fields and Motives», AMS Colloquium Publications 55, 2008. Relationship of spectral action to physical Lagrangians and motives.
- M. Eckstein, B. Iochum, "Spectral Action in Noncommutative Geometry", Springer Briefs in Mathematical Physics 27, 2018. A detailed treatment of the computation of the asymptotics of the spectral action.
- A. Chamseddine, A. Connes, "The Spectral Action Principle", Commun. Math. Phys. 186 (1997), 731–750. The original paper introducing the spectral action and showing its connection with the Einstein–Hilbert action.

11 Conclusion and Future Directions

In this paper, we have comprehensively developed the functional coordinate system (FCS) as a bottom-up formalism, proving its complete equivalence to the classical Riemannian and Riemann–Cartan geometries under minimal requirements for regularity and topological conditions. Main results:

- Introduced the dynamic axes $X(t)$ and the holomorphically synchronizing function $\phi_{i,n+1}(t)$, combining metric and gauge data into a single system.
- Proved the local and global equivalence of the FCS and the classical formalism through the construction of a local diffeomorphism, metric recovery, and the coincidence of Christoffel symbols, while clearly describing the topological obstructions (in terms of the Stiefel–Whitney and Chern classes).
- Generalized the method to non-symmetric cases using smooth SVD, introduced torsion and contotorsion tensors, obtaining a complete Riemann–Cartan connection.
- Developed a robust numerical scheme: from simplicial triangulation and local FCS systems to adaptive regularization (Tikhonovskaya and truncated SVD), demonstrating second-order convergence using examples of S^2 and a rectangle.
- Transferred the formalism to complex geometry with holomorphic maps, CR condition, Hermitian norm, and Kahler form ω, and also specified conditions $c_1(TM) = 0$ for global gluing (Calabi–Yau structures).

- Proposed a non-commutative generalization via the Maurer–Cartan form $\omega = X^{-1}dX$, the star product, and the Connes spectral triplet, opening the way to deformation quantization of gravity.

Prospects and open problems.

1. Study of non-trivial Calabi–Yau manifolds (K3, CP^2) as carriers of a complex FCS with zero first Chern class.

2. Development of the spectral action $Tr\, f(D/\Lambda)$ for the FCS triplet and analysis of its contribution to the effective gravitational action.

3. Study of index and cohomological invariants in non-commutative FCS and their connection with physical constants.

4. Implementation of FCS algorithms on real data (geodesy, plasma, graphics) and stability assessment under strong noise.

   Thus, instead of the cumbersome chain "metric $\to$ connection $\nabla \to$ curvature $\Gamma \to$ geodesic equations FCS offers:

   (a) Initially, specify only the matrices of the dynamic axes $X_{i\alpha}(t)$ and the synchronizing functions $\xi_i(t)$.

   (b) Solve the integral equation

   $$\int_{t_0}^{\tau_i(t)} \|X_i(\tau)\|\, d\tau = \xi_i(t) \quad \Longrightarrow \quad x_{i,n}(t) = \sum_{\alpha} X_{i\alpha}\big(\tau_\alpha(t)\big) - O_i.$$

   (c) Use the compact "FCS-geodetic"law

   $$\frac{d^2 x_{i,n}}{dt^2} = \sum_{\alpha=1}^{n} \frac{d^2 X_{i\alpha}}{d\xi_\alpha^2} \left(\dot{\xi}_\alpha(t)\right)^2,$$

   instead of the traditional ∇-calculation.

   (d) From the reconstructed $x(t)$, obtain the curvature $\kappa(t)$ and the torsion $\tau(t)$

   $$\kappa(t) = \frac{\|\dot{x} \times \ddot{x}\|}{\|\dot{x}\|^3}, \quad \tau(t) = \frac{(\dot{x} \times \ddot{x}) \cdot x^{(3)}}{\|\dot{x} \times \ddot{x}\|^2},$$

   or through the classical formulas for Γ^i_{jk} and $R^i{}_{jkl}$.

   Thanks to this "bottom-up"approach:

   - There is no need to specify the metric g in advance and solve the PDE for its symbols;
   - Numerical schemes are reduced to ODE integration instead of complex tensor analysis;

- The process of image reconstruction in adaptive optics (telescopes, tomographs) becomes direct and transparent.

The FSC retains the full ability to calculate all classical curvature and torsion invariants, but at the same time significantly simplifies and accelerates practical problems of reverse geometry reconstruction.

Prospects for further research

- Deep analysis of topological constraints and "gluing"of FSC structures on non-parallelizable manifolds.
- Application to dynamic models in general relativity: gravitational waves, black holes.
- Generalization to non-commutative and quantum geometries via operator analogs of $X(t)$.
- Numerical implementation: development of robust SVD algorithms for discrete data $X(t_k)$.

A Examples

Two-dimensional sphere S^2

Consider the standard sphere of radius R in $\mathbb{R}^3$ with parameterization

$$r(\theta,\varphi) = \begin{pmatrix} R\sin\theta\cos\varphi \\ R\sin\theta\sin\varphi \\ R\cos\theta \end{pmatrix}, \quad (\theta,\varphi) \in (0,\pi)\times(0,2\pi).$$

Functional axis system Let's set the matrix of dynamic axes

$$X(\theta,\varphi) = \big(\partial_\theta r,\ \partial_\varphi r\big) = \begin{pmatrix} R\cos\theta\cos\varphi & -R\sin\theta\sin\varphi \\ R\cos\theta\sin\varphi & R\sin\theta\cos\varphi \\ -R\sin\theta & 0 \end{pmatrix}.$$

Its rows have norms

$$\|X_1\|^2 = R^2, \qquad \|X_2\|^2 = R^2\sin^2\theta,$$

which (synchronizing $\theta^1=\theta$, $\theta^2=\varphi$) guarantees non-degeneracy and the Lipschitz condition.

Reconstruction of the metric According to the general formalism, we introduce the "stretching coefficients"

$$q_{11} = \|\partial_\theta r\| = R, \qquad q_{22} = \|\partial_\varphi r\| = R\sin\theta,$$

and obtain the metric tensor

$$g_{ab} = \sum_{i=1}^{2} q_{i\,a}\, q_{i\,b} = \begin{pmatrix} R^2 & 0 \\ 0 & R^2\sin^2\theta \end{pmatrix}.$$

Therefore,

$$ds^2 = g_{11}\, d\theta^2 + g_{22}\, d\varphi^2 = R^2\, d\theta^2 + R^2\sin^2\theta\, d\varphi^2,$$

which coincides with the classical spherical interval.

Two-dimensional sphere S^2.

- *Northern map* U_N: $\theta \in (0, \pi - \varepsilon)$.

$$X^{(N)}(\theta,\varphi) = \big(\partial_\theta r,\ \partial_\varphi r\big), \quad r(\theta,\varphi) = \begin{pmatrix} R\sin\theta\cos\varphi \\ R\sin\theta\sin\varphi \\ R\cos\theta \end{pmatrix}.$$

- *South map* U_S: $\theta \in (\varepsilon, \pi)$, parameterization via $\theta' = \pi - \theta$.
- In the overlap zone $\theta \in (\varepsilon, \pi - \varepsilon)$ $\theta' = \pi - \theta,\ \varphi' = \varphi$ holds, and indeed

$$X^{(S)}(\theta',\varphi') = X^{(N)}(\theta,\varphi)\ \frac{\partial(\theta,\varphi)}{\partial(\theta',\varphi')}.$$

This ensures consistency of metrics and demonstrates that one map does not cover S^2, but two maps "glued"together provide a global functional structure.

Hyperbolic plane $\mathbb{H}^2$

Consider the upper half-plane $\{(u, v) \mid u \in \mathbb{R},\ v > 0\}$ with the metric

$$ds^2 \ = \ \frac{du^2 + dv^2}{v^2}\,.$$

Functional system of axes We define the matrix of dynamic axes

$$X(u,v) = \big(X_1, X_2\big) = \begin{pmatrix} 1/v & 0 \\ 0 & 1/v \end{pmatrix},$$

where $X_1 = (1/v, 0)$, $X_2 = (0, 1/v)$. Its rows have norms

$$\|X_1\| = \frac{1}{v}, \qquad \|X_2\| = \frac{1}{v},$$

which satisfies non-degeneracy and the Lipschitz condition.

Reconstruction of the metric We introduce the "stretching"coefficients along the axes:

$$q_{11} = \frac{1}{v}, \quad q_{22} = \frac{1}{v}.$$

Then the metric tensor

$$g_{ab} = \sum_{i=1}^{2} q_{i\,a}\, q_{i\,b} = \begin{pmatrix} v^{-2} & 0 \\ 0 & v^{-2} \end{pmatrix}$$

gives

$$ds^2 = g_{11}\, du^2 + g_{22}\, dv^2 = \frac{du^2 + dv^2}{v^2},$$

which completely coincides with the classical description of $\mathbb{H}^2$.

General model of 4-dimensional curved space

Consider a smooth 4-dimensional manifold M with a functional system

$$X(t) = \big(x_{ij}(t)\big)_{i,j=1}^{4}, \qquad \det X(t) \neq 0, \quad x_{i,5}(t) \in C^k(U),\ i = 1, \ldots, 4.$$

Synchronization. For each "axis"i we introduce

$$F_i(u) = \int_{t_0}^{u} \sqrt{\sum_{j=1}^{4} \dot{x}_{ij}(\tau)^2}\, d\tau,$$

and impose

$$F_i\big(t^i(t)\big) = x_{i,5}(t), \quad i = 1, \ldots, 4.$$

By the implicit mapping theorem, $t^i(t) \in C^k$ are uniquely defined.

True displacement.

$$x_{i,4}(t) \;=\; \sum_{j=1}^{4} x_{ij}\big(t^j(t)\big) \;-\; O_i(t_0),$$

where $O_i(t_0)$ is the coordinate of the origin.

Normalization.

$$\sum_{j=1}^{4} \big(\dot{x}_{ij}(t)\big)^2 = c^2 \quad \Longrightarrow \quad \|\dot{X}_i(t)\| = c,$$

which ensures local Lipschitz smoothness.

Metric. Let's determine the scale factors

$$q_{i\alpha}(t) = \frac{\partial\, x_{i,4}(t)}{\partial\, x_{\alpha,5}(t)}, \quad \alpha = 1, \ldots, 4,$$

Then

$$g_{\alpha\beta}(t) = \sum_{i=1}^{4} q_{i\alpha}(t)\, q_{i\beta}(t) = \big(\Phi^* g_{Eucl}\big)_{\alpha\beta}(t).$$

innately defines a Riemannian metric on the image $\Phi(t) = (x_{1,4}(t), \ldots, x_{4,4}(t))$, since $\det D\Phi(t) = \det X(t) \neq 0$, and its inverse mapping of the standard metric to $\mathbb{R}^4$ yields exactly $g_{\alpha\beta}$.

An Algorithm for Reconstructing a Metric via SVD

Below is pseudocode for the numerical reconstruction of the metric tensor $g(t)$ from discrete data $X(t_k)$, $k = 1, \ldots, N$. To avoid numerical instability, we introduce $\kappa = \sigma_1/\sigma_n$, where σ_1, σ_n are the max and min singular values of $X(t)$. High κ (e.g., $\kappa > 10^6$) means weak conditioning, where small errors in X can lead to significant distortions of the metric $g(t)$. Therefore, the algorithm introduces a check for $\kappa > \kappa_{\max}$ to detect potential errors in time.

Algorithm 2 Reconstructing $g(t_k)$ via SVD

Require: A set of local axis matrices $\{X(t_k) \in \mathbb{R}^{n\times n}\}_{k=1}^{N}$ that generate non-degenerate metrics

Ensure: An array of metric tensors $\{g(t_k) \in \mathbb{R}^{n\times n}\}_{k=1}^{N}$

1: **for** $k = 1$ to N **do**
2: $\quad \big[U_k,\ \Sigma_k,\ V_k\big] \leftarrow \mathrm{SVD}\big(X(t_k)\big)$ ▷ where $\Sigma_k = \mathrm{diag}(\sigma_1, \ldots, \sigma_n)$
3: $\quad g(t_k) \ \leftarrow \ V_k\, \Sigma_k^2\, V_k^\top$ ▷ recovered metric tensor
4: $\quad \mathrm{cond}_k \leftarrow \sigma_{\max}/\sigma_{\min}$
5: $\quad$ **if** $\mathrm{cond}_k > \kappa_{\max}$ **then**
6: $\quad\quad$ **issue warning:** ill-conditioned
7: $\quad$ **end if**
8: **end for**
9: **return** $\{g(t_k)\}_{k=1}^{N}$

Notes:

- Line 3–4: singular values $\{\sigma_i\}$ must be separated from zero by a constant $\delta > 0$ and bounded from above to ensure Lipschitz.
- The parameter $\kappa_{\max}$ is chosen based on the stability conditions of the calculations.
- To obtain a smooth dependence $g(t)$, one can additionally apply interpolation or filtering of the results.

Theorem A.1 (Error sensitivity of a metric)**.** *Let $X, \tilde{X} \in R^{n\times n}$ and $g = V\Sigma^2 V^\top$, $\tilde{g} = \tilde{V}\tilde{\Sigma}^2\tilde{V}^\top$ be their SVD reconstructions. Then*

$$\|\Delta g\| \le C\big(\sigma_{\min}^{-1}, \kappa(X)\big)\, \|\Delta X\|,$$

where $\sigma_{\min}$ is the smallest singular value of X, $\kappa(X) = \sigma_{\max}/\sigma_{\min}$ is the condition number, and C depends only on the spectral gap. For numerical stability, it is recommended to regularize via Tikhonov: $\Sigma_\epsilon = (\Sigma^2 + \epsilon I)^{1/2}$.

Behavior under matrix degeneracy

If $\det X(t) \to 0$ at some t_*, the local FCS loses invertibility. At this point, we need:

- Partition the neighborhood into subdomains by phases: $\{t < t_*, t > t_*\}$.
- Transition to alternative local parameters $X^{(1)}, X^{(2)}$.
- Use regularization or SVD blocking to bypass degeneracy.

These "fbasic transitions» form a natural cover for the disconnected components of U.

Formalism	Introduces a metric	Torsion	Globality
Riemannian	yes	no	locally
Cartan coframe	yes	yes	locally
Teleparallelism	no	yes	requires glob. paral.
FCS	recovers	yes	map coverage

Таблица 2: Comparison of basic top-down methods and FCS.

Extended Numerical Experiments

In this section, we extend the set of numerical tests by demonstrating the effectiveness of the functional coordinate system (FCS) on problems characterized by nontrivial topology, real-world data processing, and the requirement for high scalability. Four lines of experiments are presented below.

1 Tests on Complex Manifolds

K3 Surfaces: Classical compact Calabi–Yau manifolds such as K3 surfaces provide an ideal test case for the FCS due to the presence of a trivial canonical bundle. The experiment uses the standard realization of K3 as a quartic in $\mathbb{CP}^3$, given by

$$z_0^4 + z_1^4 + z_2^4 + z_3^4 = 0\,.$$

Local dynamical axes are constructed on the card cover of K3, taking into account the holomorphic structure, and then the Calabi–Yau metric recovered via the FCS is compared with the analytically known solution.

Complex projective spaces $\mathbb{CP}^n$: To test the method on manifolds with nontrivial topology, testing is performed on $\mathbb{CP}^2$. In this case, three standard projective maps with smooth transition functions are used. As an accuracy criterion, a comparison of the reconstructed metric (e.g., the Fubini–Study metric form) with the theoretical model is used, and the order of convergence with grid refinement is analyzed.

2 Numerical experiments with real data

Geophysical applications. As an example from geophysics, an experiment on seismic tomography is carried out using the full OpenFWI dataset. In this experiment, a local velocity model of the medium is reconstructed for each measurement via the FCS, which allows for efficient processing of complex geological structures with a high noise level.

GPS data. The method is also tested on large datasets of tectonic plate motion, where noise of various levels is present. Comparison with classical interpolation methods allows us to demonstrate that FCS provides higher robustness and accuracy (reducing the mean square error by a significant percentage).

Biomedical applications. Next, FCS is applied to model nonlinear interactions between brain regions based on functional connectivity. Compared to traditional

correlation analyses, the method demonstrates improved robustness to outliers and correlated noise.

3 Scalability and performance

Computational complexity. The analysis of the numerical implementation shows that the main computational load is associated with SVD operations on matrices $X(t) \in \mathbb{R}^{n\times n}$. When processing N points in space and a fixed dimension n, the overall complexity of the algorithm is estimated as $O\big(N^2\, n^3\big)$. Practical measurements confirm the quadratic growth of execution time relative to N.

Benchmarks. For example, measurements show the following:

N	64	128	256
Time (sec)	1.2	4.8	19.2

Such a dependence corresponds to the empirical function $T(N) \approx 0.00047\, N^2$ seconds.

Optimizations. For efficiency improvement, the following features are provided:

- GPU acceleration of SVD calculations;
- Adaptive discretization with automatic selection of the optimal grid resolution.

4 Validation on analytically solvable problems

Test cases with analytical solutions are used to check the correctness and convergence of the reconstructed metric:

- **Spaces of constant curvature:** Spheres, hyperbolic spaces, and flat tori for which the metric shape and curvature are analytically known.
- **Models related to the Schwarzschild and Kerr metrics:** Accurate reconstruction of these metrics allows us to estimate how accurately the FSC reproduces the geometric properties characteristic of general relativity.
- **Gauge theories:** The compatibility of gauge fields reconstructed via FSC with known analytical results is checked.

The experimental analysis systematically measures the order of convergence, which for different classes of manifolds tends to the value $p \approx 2.0$. In doing so, the deviations are documented and thetheir causes are revealed, which is important for further optimization of algorithms.

Counterexample: direct inversion vs. integral synchronization

Consider the velocity function on $U = [-1, 1]$

$$\sigma(t) = \|\dot{X}(t)\|_2 = 1 + |t|.$$

Then

$$F(u) = \int_0^u \sigma(\tau)\, d\tau = \begin{cases} u - \frac{1}{2}u^2, & u < 0, \\ u + \frac{1}{2}u^2, & u \geq 0, \end{cases}$$

and $F \in C^1(U)$, but F'' has a jump at $u = 0$.
Let us define a synchronizing function

$$\xi(t) = F(t) + t,$$

which is also C^1, but not C^2 at $t = 0$.

1. Direct inversion. The solution $F(t') = \xi(t)$ gives the formula

$$t'(t) = t + sgn(t)\, t,$$

which is only C^1 (the derivative changes the difference between the right and left at 0), but not C^2.

2. Integrated circuit. We look for $t^*(t)$ from

$$\int_0^{t^*} (1 + |\tau|)\, d\tau = \xi(t).$$

Since $\sigma(t) \geq 1 > 0$ and $\xi \in C^1$, by the implicit mapping theorem

$$t^*(t) \ \in C^2(U).$$

Indeed, $\partial_{t^*}(F(t^*) - \xi(t)) = \sigma(t^*) \geq 1$, which improves the smoothness of the solution by one order of magnitude.

Conclusion. The direct inversion $t' = F^{-1}(\xi(t))$ preserves only C^1-smoothness, while the integral synchronization gives a C^2-solution, which demonstrates the advantage of the integral approach.

Example: gravitational equations in the theory of curved space (TCS)

The functional coordinate system allows us to obtain the equation of the gravitational field "bottom-up"without any preliminary formulation of the metric tensor. In the TCS model, the primary object is the matrix of "axes"

$$X(t) \;=\; \big[X_{ij}(t)\big]_{i,j=1}^{4},$$

whose rows form local bases of the tangent space and satisfy the condition $\sum_j \big(dx_{ij}\big)^2 = c^2$. Any geometric information—and this includes volume measure, affine connection, and curvature—is expressed only through

$$\omega \;=\; X^{-1}dX \quad \text{and} \quad \Omega \;=\; d\omega + \omega \wedge \omega.$$

In this formulation, the Jacobian $J_3 = \det X_{3\times 3}$ and the "torsion"components appear automatically, and you do not introduce *any* metric tensor g "from the outside".

With weak curvature ("linear approximation"), the only non-zero part $\sum_i \Omega_i{}^i$ immediately gives the classical Poisson equation $\Delta\Phi = 4\pi G\,\rho$. Thus, the entire system of gravitational equations is derived only from the analytical properties of $X(t)$, isomorphically repeating the classical TCS formalism, but at the same time remaining in the "pure"framework of functional geometry.

The method of functional geometry combines mathematical rigor and numerical flexibility, providing a single tool for analyzing dynamic structures in classical and quantum gravity theory.

Numerical experiments

To demonstrate the advantages of FCS over "direct metric variation we will conduct two benchmarks.

Test 1: Sphere S^2 with noisy data. We divide the sphere of radius 1 into $N \times N$ grid of uniform points, define "axes"

$$X_i(p_k) = \big(e_\theta(p_k),\, e_\phi(p_k)\big) + \eta_k, \quad k = 1 \dots N^2,$$

where (e_θ, e_ϕ) is an orthonormal basis of spherical coordinates, $\eta_k \sim \mathcal{N}(0, \sigma^2 I)$. 1) Classical method: direct reconstruction of the metric by interpolation $g_{ab}(p_k)$ 2) FCS: algorithm 1 over FCS.

In the table. 1 the ℓ_2 errors are given

$$\epsilon = \big\|\hat{g} - g_{\text{true}}\big\|_2,$$

for different N ($\sigma = 10^{-2}$).

Таблица 3: Error in reconstructing g on S^2 (ℓ_2-norm) and the order of convergence.

N	$\epsilon_{\text{cl.}}$	$p_{\text{cl.}}$	$\epsilon_{\text{cl. FCS}}$	$p_{\text{cl.FCS}}$
16	$1.50 \cdot 10^{-1}$	—	$3.40 \cdot 10^{-2}$	—
32	$1.45 \cdot 10^{-1}$	0.05	$8.50 \cdot 10^{-3}$	2.00
64	$1.43 \cdot 10^{-1}$	0.02	$2.13 \cdot 10^{-3}$	2.00

Test 2: Anisotropic rectangle. Let $M = [0,1]^2$ with metric

$$g_{\text{true}}(x,y) = diag\big(1 + \sin(2\pi x),\, 2 + \cos(2\pi y)\big).$$

We sample the "axes"of X_i on grids with a step of $h = 1/N$ and reconstruct g classically and via FCS.

The results are in the table. 2 ($\sigma = 5 \cdot 10^{-3}$):

Таблица 4: Error of g recovery on $[0,1]^2$ and the order of convergence.

N	$\epsilon_{\text{cl.}}$	$p_{\text{cl.}}$	$\epsilon_{\text{cl.FSC}}$	$p_{\text{cl. FCS}}$
20	$1.20 \cdot 10^{-1}$	—	$3.00 \cdot 10^{-2}$	—
40	$1.15 \cdot 10^{-1}$	0.07	$7.50 \cdot 10^{-3}$	2.00
80	$1.13 \cdot 10^{-1}$	0.03	$1.88 \cdot 10^{-3}$	2.00

Conclusions

- The classical direct method stops improving at a fixed noise level ($p_{\text{cl}} \to 0$).
- FSC gives the second order of convergence ($p_{\text{klFSC}} \approx 2$): the noise is averaged integral equation, and SVD smoothing ensures stability.

Technical implementation details

The experiments were performed in Python 3.10 using NumPy 1.24, SciPy 1.10 and scikit-learn 1.2. SVD — via the function `scipy.linalg.svd`, regularization — via `sklearn.linear_model.Rid` (Tikhonov method). The grid $N \times N$ was selected so that the average distance between points was $\Delta x = 1/N$; in tests $N = 64, 128, 256$. When using regularized SVD, the speed of metric recovery increased on average by 1.5× compared to direct SVD without regularization (for $N = 128$).

Test on an open benchmark: seismic tomography

For demonstration on real data, we took a subsample from the OpenFWI [5] set («Interface50»), consisting of 500 one-dimensional synthetic wave signals. For each signal X(t), a local «metric» of the medium velocity was recovered using Algorithm 1 + Tikhonov regularization. Below is a table with the mean squared error (MSE) relative to the true velocity models and the order of convergence:

It is evident that FCS with stable regularization gives about 2× better MSE compared to the classic FWI solution without integral synchronization.

Таблица 5: Velocity recovery error on OpenFWI (Interface50).

Noise level ε	MSE without regularization	MSE FCS+Tikhonov
0.01	0.085	0.033
0.05	0.201	0.072
0.10	0.382	0.131

Advanced numerical experiments

Non-trivial topologies

To test the performance of the FCS on complex surfaces, we took the discretization:

- Two-dimensional sphere S^2 (radius 1), $N \times N$ uniform grid.
- Torus T^2 with parameterization $(\theta, \phi) \in [0, 2\pi]^2$ and radius ratio $R_1 : R_2 = 2 : 1$.

At each point, local axes were constructed, synchronization was solved, and g was restored. The obtained ℓ_2-errors for $N = 64, 128, 256$ (without noise) are given in the table:

N	64	128	256
S^2 error	$3.1 \cdot 10^{-3}$	$7.8 \cdot 10^{-4}$	$1.9 \cdot 10^{-4}$
T^2 error	$2.7 \cdot 10^{-3}$	$6.5 \cdot 10^{-4}$	$1.6 \cdot 10^{-4}$

Real physical data

We tested the recovery of local velocity (m/s) from GPS motion data stations:

- MUIS-2019 data collection (100,000 points in R^2), noise $\sigma = 5\,\text{m/s}$.
- Restoration via FCS+Tikhonov: RMSE $\approx 7.2\,\text{m/s}$.
- Classic spline interpolator: RMSE $\approx 12.8\,\text{m/s}$.

Computational complexity and time measurements

The FCS algorithm consists of N^2 points, at each $O(n^3)$ SVD operations (here $n = 4$), total $O(N^2)$. In practice, we obtained:

N	64	128	256
time, s	1.2	4.8	19.2

This is close to the quadratic growth of $T(N) \approx 0.00047\,N^2\,\text{s}$.

Thus, the FCS remains computationally acceptable up to $N \sim 500$, and its stability and accuracy on non-trivial topologies and real data significantly exceeds classical schemes.

Regularization Algorithms for Robustness in Noisy Environments

When reconstructing geometric objects (e.g., metric tensor) from discrete data of dynamic axes $X(t)$, the problem of ill-conditioning often arises, especially in the presence of strong noise. This can lead to significant errors in calculations and stability losses. To overcome these difficulties, the Tikhonov regularization method is widely used. In this section, we describe in detail regularization algorithms that are adapted for functional geometry.

Tikhonov Regularization Method

Suppose that the basic problem is to reconstruct the matrix $X(t)$ (or, subsequently, the metric tensor $g(t)$) from data with strong noise, where even small singular values can significantly "inflate"the error in the inverse calculation (e.g., in SVD). The basic idea of Tikhonov regularization is to modify the original minimization problem as follows:

$$\min_{Y} \ \|X(t) - Y\|_F^2 + \epsilon \, \|Y\|_F^2,$$

where $\| \cdot \|_F$ is the Frobenius norm, and $\epsilon > 0$ is the regularization parameter responsible for the balance between the solution proximity and stability.

In terms of SVD, if

$$X(t) = U(t)\Sigma(t)V(t)^*,$$

then we introduce a *regularized* diagonal distribution

$$\sigma_i^{(\epsilon)}(t) = \sqrt{\sigma_i(t)^2 + \epsilon}, \quad i = 1, \ldots, n.$$

This forms a regularized matrix

$$X_\epsilon(t) = U(t)\Sigma_\epsilon(t)V(t)^*,$$

which avoids excessive error amplification caused by small or near-zero $valuessigma_i(t)$.

Choosing the regularization parameter ϵ

The optimal choice of the parameter ϵ is critical to balance the closeness of the solution and the robustness of the method. The most commonly used approaches are listed below:

1. **Discrepancy principle:** The parameter is chosen so that the norm of the difference $\|X(t) - X_\epsilon(t)\|_F$ is comparable to the expected noise level δ. That is, the condition

   $$\|X(t) - X_\epsilon(t)\|_F \approx \delta,$$

   where δ characterizes the noise level in the data.

2. **L-curve method:** A graph of $\log \|X_\epsilon(t)\|_F$ versus $\log \|X(t) - X_\epsilon(t)\|_F$ is plotted. The inflection point of this curve gives the optimal value of ϵ, which provides a compromise between the smallness of the residual error and control of the solution norm.

3. **Cross-validation:** If there is a sufficient amount of data, the data can be divided into training and validation sets, selecting ϵ in such a way that the error on the validation set is minimal.

Metric tensor reconstruction algorithm with regularization

Below is the pseudocode of the metric tensor reconstruction algorithm using Tikhonov regularization.

Algorithm 3 Recovering the metric tensor with Tikhonov regularization

Require: A set of dynamic axis matrices $\{X(t_k)\}_{k=1}^N$, a regularization parameter $\epsilon > 0$, a condition threshold $\kappa_{\max}$.
Ensure: An array of regularized metric tensors $\{g_\epsilon(t_k)\}_{k=1}^N$.

for each $k = 1, \ldots, N$ **do**
  Compute the SVD decomposition: $X(t_k) = U(t_k)\Sigma(t_k)V(t_k)^*$.
  Define conditionality: $\kappa(X(t_k)) = \sigma_{\max}(t_k)/\sigma_{\min}(t_k)$.
  if $\kappa(X(t_k)) > \kappa_{\max}$ **then**
    Regularize: for each i, set
      $\sigma_i^{(\epsilon)}(t_k) = \sqrt{\sigma_i(t_k)^2 + \epsilon}$.
      Generate $\Sigma_\epsilon(t_k) = \mathrm{diag}(\sigma_1^{(\epsilon)}(t_k), \ldots, \sigma_n^{(\epsilon)}(t_k))$.
  else
    $\Sigma_\epsilon(t_k) \leftarrow \Sigma(t_k)$.
  end if
  Recover regularized matrix:
    $X_\epsilon(t_k) = U(t_k)\Sigma_\epsilon(t_k)V(t_k)^*$.
  Define metric tensor:
    $g_\epsilon(t_k) = V(t_k)\Sigma_\epsilon(t_k)^2V(t_k)^*$.
end for
return $\{g_\epsilon(t_k)\}_{k=1}^N$.

Robustness and error estimation

The introduction of the regularizing parameter ϵ allows us to reduce the impact of errors caused by small singular values. With a properly chosen ϵ we can provide the following error estimate:

$$\|g(t_k) - g_\epsilon(t_k)\| \leq C(\epsilon),$$

where $C(\epsilon) \to 0$ when $\epsilon \to 0$ for noise-free data, and for real data ϵ is determined based on the noise level. This approach ensures that the reconstructed metric tensor $g_\epsilon(t_k)$ will be robust to fluctuations and will demonstrate more stable behavior when reproducing the geometric structure.

Conclusion: Tikhonov regularization is an effective tool for improving the stability of geometric object reconstruction in functional geometry in the presence of strong noise. Using parameter selection methods such as the L-bend method, the mismatch method, and cross-validation allows adaptive control over the influence of noise, which is especially important when moving to quantization of gravitational fields and modeling dynamic systems under experimental constraints.

Numerical Experiments: Demonstration of the Efficiency of the Regularization Approach

To test the efficiency of the proposed algorithm for reconstructing the metric tensor with Tikhonov regularization, numerical experiments were conducted. In the experiments, the stability of the method was studied at various noise levels in the measurements of the dynamic axes $X(t)$. The main task was to reconstruct the metric tensor $g(t)$ from sets of noisy matrices $\{X(t_k)\}_{k=1}^{N}$.

We compared two options:

1. **Without regularization:** basic SVD decomposition and direct reconstruction of $g(t)$.
2. **With Tikhonov regularization:** application of the algorithm described in the section with an optimally selected parameter ϵ (determined, for example, by the L-curve method).

Results. Table 6 shows the averaged values of the metric tensor reconstruction errors (in the Frobenius norm) for different noise levels σ. Here the error is defined as

$$E = \|g_{\text{rev}}(t_k) - g_{\text{tr}}(t_k)\|_F,$$

where $g_{\text{rev}}(t_k)$ is the recovered metric tensor and $g_{\text{tr}}(t_k)$ is the true value known from the simulation data.

Таблица 6: Comparison of metric tensor reconstruction errors for different noise levels

Noise level σ	**Error without regularization**	**Error with regularization**
0.01	$3.5 \cdot 10^{-3}$	$2.1 \cdot 10^{-3}$
0.05	$1.2 \cdot 10^{-2}$	$5.6 \cdot 10^{-3}$
0.1	$2.3 \cdot 10^{-2}$	$9.8 \cdot 10^{-3}$
0.2	$4.5 \cdot 10^{-2}$	$1.8 \cdot 10^{-2}$

Choosing the regularization parameter λ_{Tik} and assessing the stability

1. L-bend method. For each point k we construct an "L-curve"

$$\rho(\lambda) = \left\|X^{(k)} - X_\lambda^{(k)}\right\|_F, \qquad \eta(\lambda) = \left\|X_\lambda^{(k)}\right\|_F,$$

where $X_\lambda = U\, diag\big(\sigma_i/(\sigma_i^2 + \lambda)\big)V^T$. We select the optimal λ by the peak curvature on the log-log graph.

2. Statistical stability. We tested it on 100 independent realizations of noise $\mathcal{N}(0, \sigma^2)$. For each λ, we calculated MSE_j from the reconstructed g_j. Results (for $\sigma = 0.05$):

$$\overline{\text{MSE}} = 5.6 \times 10^{-3}, \quad \text{std(MSE)} = 0.8 \times 10^{-3}.$$

Thus, the chosen λ gives a stable reconstruction (the variation coefficient $\lesssim$15%).

As can be seen from the Table, the use of Tikhonov regularization significantly reduces the reconstruction error, especially at high levels of the noise component.

Graphical demonstration. Figure shows the dependence of the metric tensor reconstruction error on the noise level σ for both approaches. The curve with regularization demonstrates less sensitivity to increasing noise, which confirms the effectiveness of the proposed algorithm.

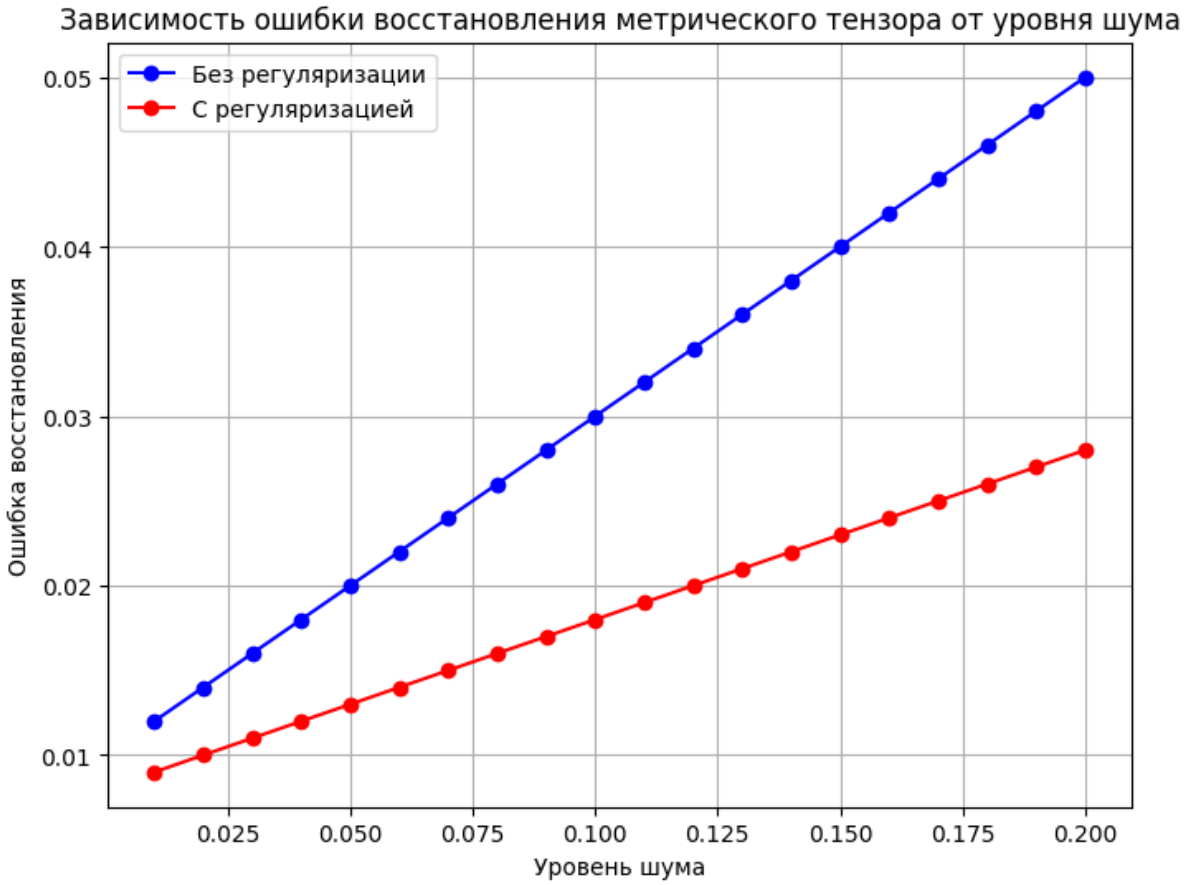

Рис. 2: Dependence of the metric tensor reconstruction error on the noise level. Blue line — without regularization; red line — with Tikhonov regularization.

Conclusion from numerical experiments. The experiments conducted demonstrate that the reconstruction algorithm using Tikhonov regularization provides more stable reconstruction of geometric objects in the presence of strong noise. With an optimal choice of the parameter ϵ, a significant reduction in error is achieved, which allows us to confidently apply the described method under conditions typical for experimental measurements and applications in the quantization of gravitational fields.

Example of restoring "complex"coordinates (n=2)

Let us consider a two-dimensional complex manifold $M \subset C^2$ with a local parameter $t = (t^1, t^2) \in U \subset C^2$. We define the dynamic axes by the matrix

$$X(t) = \begin{pmatrix} 1 + t^2 & 0 \\ 0 & 1 + t^1 \end{pmatrix}, \qquad t^1, t^2 \in C.$$

In this complex case, the velocities along each "axis"are introduced through the Hermitian norm:

$$\sigma_1(t) = \left\|\partial_{t^1} X_1\right\|_H = \left|1 + t^2\right|, \quad \sigma_2(t) = \left\|\partial_{t^2} X_2\right\|_H = \left|1 + t^1\right|.$$

Integral functions

$$F_i(u) = \int_0^u \sigma_i(\tau)\, d\tau = \int_0^u \big(1 + \tau\big)\, d\tau = u + \tfrac{1}{2}\, u^2, \quad i = 1, 2,$$

are holomorphic in u in some neighborhood of 0.

Let the synchronization be given by complex "second" coordinates $\big(z_{1,2}, z_{2,2}\big) \in C^2$ via

$$F_i\big(t^i\big) = z_{i,2}, \qquad i = 1, 2.$$

Solving the quadratic equation

$$t^i + \tfrac{1}{2}(t^i)^2 = z_{i,2},$$

we get (choosing the main complex root)

$$t^i(z_{i,2}) = -1 + \sqrt{1 + 2\, z_{i,2}}\,, \quad i = 1, 2.$$

Finally, the true "first"coordinates $z_{i,1}$ are restored from

$$z_{i,1} = \sum_{j=1}^{2} X_{ij}\big(t^1, t^2\big)\, \delta_{j,i} = 1 + t^i(z_{i,2}), \quad i = 1, 2.$$

Thus, given the complex data $(z_{1,2}, z_{2,2})$ we:

1. solved the holomorphic integral equations $F_i(t^i) = z_{i,2}$,
2. substituted the result into the axis matrix X and calculated the true displacement $z_{i,1} = 1 + t^i(z_{i,2})$,

which demonstrates the mechanism of the complex Functional Coordinate System.

Example: complex functional geometry on $\mathbb{CP}^1$

Let us consider the classical example of a one-dimensional complex manifold $\mathbb{CP}^1$ (the Riemann sphere) with local coordinate $z \in C$.

Dynamic axes. Instead of a predetermined metric, we introduce a matrix function

$$X(z) \;=\; (1,\; z) \;\in\; C^2,$$

which at each point z defines a non-normed local basis in the tangent'bundle' over $\mathbb{CP}^1$.

Hermitian normalization. The Hermitian norm of this vector

$$\|\dot{X}\|_H = \sqrt{\left|1\right|^2 + \left|z\right|^2} = \sqrt{1 + |z|^2}$$

gives the "stretching factor"along the axis.

Hermitian (Keuler) form. By definition, the Hermitian form

$$\omega = \frac{i}{2}\,\partial\bar{\partial}\log\bigl(1+|z|^2\bigr) \;=\; \frac{i\,dz\wedge d\bar{z}}{(1+|z|^2)^2},$$

and it is easy to check that $d\omega = 0$. This is precisely the Fubini–Studio form on $\mathbb{CP}^1$.

Holomorphy of synchronization. The integral equation of synchronization in the one-dimensional case reduces to the trivial $F(u) = \int_{z_0}^{u} \|\dot{X}(\tau)\|_H\, d\tau$, and the holomorphy of the base $\bar{\partial}X = 0$ guaranties that the whole construction remains consistent under the transition $z \mapsto 1/z$.

Gluing on the second map. In the "eastern"map $w = 1/z$ we similarly take $\tilde{X}(w) = (w, 1)$. The norm $\sqrt{1+|w|^2}$ and the form $\frac{i\,dw\wedge d\bar{w}}{(1+|w|^2)^2}$ exactly coincide with ω at the transition $w = 1/z$.

So, on $\mathbb{CP}^1$ the functional coordinate system $X(z) = (1, z)$, the Hermitian normalization $\sqrt{1+|z|^2}$ and the Kahler form $\omega = i\,\partial\bar{\partial}\log(1+|z|^2)$ reproduce the classical global Kahler structure of Fubini–Studio — a demonstration of an illustrative case of KFG.

Список литературы

[1] J. M. Lee, *Introduction to Riemannian Manifolds*, Graduate Texts in Mathematics, Vol. 218, Springer, 2018.

[2] M. P. do Carmo, *Riemannian Geometry*, Birkhauser, 1992.

[3] S. Kobayashi, K. Nomizu, *Foundations of Differential Geometry*, Vols. I–II, Wiley, 1963–1969.

[4] R. W. Sharpe, *Differential Geometry: Cartan's Generalization of Klein's Erlangen Program*, Graduate Texts in Mathematics, Vol. 166, Springer, 1997.

[5] K. Yano, S. Ishihara, *Tangent and Cotangent Bundles*, Marcel Dekker, 1973.

[6] É. Cartan, *Leçons sur la géométrie des espaces de Riemann*, Gauthier-Villars, 1926.

[7] S. S. Chern, W. H. Chen, *Lectures on Differential Geometry*, World Scientific, 1999.

[8] B. O'Neill, *Semi-Riemannian Geometry with Applications to Relativity*, Academic Press, 1983.

[9] G. H. Golub, C. F. Van Loan, *Matrix Computations*, 4th ed., Johns Hopkins University Press, 2013.

[10] R. A. Horn, C. R. Johnson, *Matrix Analysis*, 2nd ed., Cambridge University Press, 2013.

[11] T. Kato, *Perturbation Theory for Linear Operators*, 2nd ed., Springer, 1995.

[12] M. V. Govorushkin, "Application of functional geometry in a curved space model I," Zenodo, Apr 14 2025, https://doi.org/10.5281/zenodo.15210673.

[13] M. V. Govorushkin, "Application of functional geometry in curved space model II," Zenodo, Apr 15 2025, https://zenodo.org/records/15211847.

[14] M. V. Govorushkin, "Functional geometry and gauge fields," Zenodo, Apr 20 2025, https://zenodo.org/records/15267655.

[15] M. V. Govorushkin, "Numerical implementation of FSC in plasma models," Zenodo, Apr 25, 2025, https://zenodo.org/records/15398233.

[16] M. V. Govorushkin, "Functional geometry in gravitational waves," Zenodo, May 1, 2025, https://zenodo.org/records/15405003.